Rijksdienst voor Ondernemend Nederland

Efficiënt zonne-energie omzetten / Efficient solar conversion

EOS-LT WAELS B1 Final report

Datum Oktober 2008

ECN, H.A. Zondag, M. Bakker, V.M. van Essen, L.P.J. Bleijenendaal

In opdracht van SenterNovem (nu Rijksdienst voor Ondernemend Nederland)

Publicatienr RVO-154-1501/RP-DUZA
www.rvo.nl
Dit rapport is tot stand gekomen in opdracht van het ministerie van Economische Zaken.

ECN-I--07-000

Efficient solar conversion

More efficient conversion with conventional techniques

WAELS B1 Final report

Author(s)

H.A. Zondag, M. Bakker, V.M. van Essen, L.P.J. Bleijendaal

OCTOBER 2008

Acknowledgement/Preface
This report is a deliverable of the WAELS project. This project has received financial support from the Dutch Ministry of Economic Affairs by means of the EOS support scheme.

Abstract
PV-Thermal collectors are solar collectors that produce both electricity and heat from the same absorber area. These collectors are seen as a promising technique for the future. In this report, various options are examined to go to the next phase of PVT manufacturing, taking as a reference the flat-plate PVT module produced for the RES project. An inventory is presented of the various directions in which PVT modules could be improved and estimates are given for the potential of these options. Investigated issues are

- Improved cell absorption
- Thin film options
- Reduced glazing reflection
- Glass coatings to reduce radiative loss
- Unencapsulated cells for reduction of radiative loss
- Multicoatings for good absorption, electrical insulation and optimal heat transfer

A number of recommendations are made to improve the design, such as the use of textured c-Si cells, highly transparent glazing and multicoatings. The benefits of low emissivity coatings, unencapsulated cells and thin-film PV are less clear, and reliability issues require further testing.

Contents

List of tables

List of figures

Summary

PV-Thermal collectors are solar collectors that produce both electricity and heat from the same absorber area. These collectors are seen as a promising technique for the future. In this report, various options are examined to go to the next phase of PVT manufacturing. An inventory is presented of the various directions in which PVT modules could be improved and estimates are given for the potential of these options. Investigated issues are

- Improved cell absorption
- Thin film options
- Reduced glazing reflection
- Glass coatings to reduce radiative loss
- Unencapsulated cells for reduction of radiative loss
- Multicoatings for good absorption, electrical insulation and optimal heat transfer

A number of recommendations are made to improve the design, such as the use of textured c-Si cells, highly transparent glazing and multicoatings. The benefits of low emissivity coatings, unencapsulated cells and thin-film PV are less clear, and reliability issues require further testing.

1. Introduction

The work in WAELS B consists of two separate approaches:

- B1: Medium-term research to improve the efficiency of solar energy conversion using conventional technology (PV and solar thermal)
- B2: Long-term research into new solar thermal collector concepts that can lead to a breakthrough in the price/performance ratio.

This report is the final report of the B1 section. In this report, the focus is on the performance optimization of PV-Thermal collectors. PV-Thermal collectors are collector with solar cells on the absorber, thereby converting solar irradiance into both thermal and electrical energy simultaneously. For further optimization of their performance, the following topics were investigated.

- Improved cell absorption
- Thin film options
- Reduced glazing reflection
- Glass coatings to reduce radiative loss
- Unencapsulated cells for reduction of radiative loss
- Multicoatings for good absorption, electrical insulation and optimal heat transfer

The present work focuses on PV-Thermal. The reason for this is that PV-Thermal is seen as the most promising technique for future application, since it is an efficient way to combine the conversion of solar energy into thermal and electrical energy. However, the present generation of PVT modules show a relatively low thermal performance, which is an obstacle to the efficient use of these collectors. Therefore, it is seen as important to optimize the thermal performance of these modules further, without compromising too much the electrical efficiency of the modules. At present, important bottlenecks in the thermal performance of PVT collectors are given by

- A relatively low absorption, due to the fact that conventional PV is not optimized for absorption over the entire solar spectrum.
- Large radiative losses, due to the fact no spectrally selective coating is used.
- A relatively hot PV module, due to the fact that the heat transfer between the PV and the absorber is not optimized due to the present day use of additional layers of EVA and Clear Tedlar. In addition, the use of Clear Tedlar also contributes significantly to the cost of the modules.

All these issues are addressed in the following chapters:

- In chapter 2, an overview will be given of the potential to improve on the absorption of PV. This chapter will present research carried out at the EUT, including a summary of the results from the work of Santbergen. Also, calculations on the use of antireflective highly transparent glazing will be provided.
- In chapter 3, a thin film CIS module concept combined with antireflective glazing is considered. For this, CIS is taken as being the most promising thin-film concept due to its high solar absorption and its high electrical efficiency.
- In chapter 4, an overview will be given of the work at the EUT on antireflective coatings on glass and their potential to reduce reflection losses, as well as low-emissivity coatings and their potential for reducing the radiative losses. An important point in this work is the fact that low-emissivity coatings also provide additional absorption and reflection in the solar part of the spectrum, which should not offset the benefits from the lower radiative losses.
- In chapter 5, the theoretical potential using unencapsulated cells in a protective gas atmosphere is investigated, to reduce the radiative losses.
- In chapter 6, results will be presented on optimizing the heat transfer from the PV to the absorber by means of a low-cost multicoating concept.

2. Improved absorption

2.1 Introduction

A typical configuration for a PV-Thermal (PVT) collector is shown in Figure 1a. The prime characteristic of a PVT collector is that the solar irradiance is absorbed by the PhotoVoltaic laminate to generate both electricity and heat. The composition of the PV laminate is shown in detail in Figure 1b, in which it can be seen that the PV laminate consists of a silicon wafer with a front side texture, antireflective coating, encapsulated with EVA to a top glass and having a silvered top contact grid and an aluminum rear contact. Below the opaque aluminum rear contact, another layer of EVA connects the cells to a metallic conductor (see Figure 1a). Absorption of solar irradiance in the solar cells is crucial both for the electrical and for the thermal performance of the cells; all energy that is not absorbed is lost for the useful output of the PVT module. In order to assess the options for improving the absorption, first a general introduction for absorption in the silicon cells will be presented.

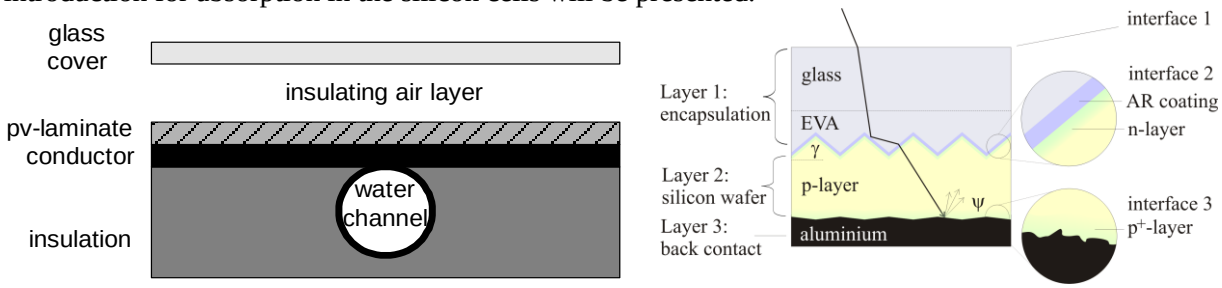

Figure 1: (a) Typical PVT collector configuration, (b) typical PV laminate configuration

The absorption in the silicon cells is determined by the fact that these cells are semiconductors. In semiconductors, a threshold energy exists above which the absorption is very efficient, but below which the material is largely transparent. The absorption coefficient of crystalline silicon is shown in Figure 2; the bandgap for crystalline silicon is about 1.1 micron. The figure clearly shows that the absorption for longer wavelengths is strongly reduced. Furthermore, this figure shows that if the silicon (which is column 4 in the periodical system) is doped by column 3 or column 5 elements (resulting in respectively p-type and n-type silicon), the absorption below the bandgap is increased, which is due to the absorption by the free carriers (electrons or holes) that result from the doping. The magnitude of this effect depends on the dopant concentration, which is reflected in the fact that free carrier absorption is much more important in the emitter (with a very high dopant condentration) than in the bulk (with a low dopant concentration).

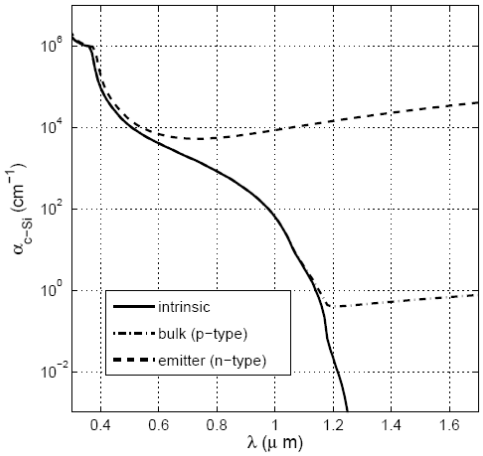

Figure 2: Absorption coefficient of crystalline silicon (indicating both absorption for pure silicon and for doped silicon as present in the bulk and the emitter of the cell).

In solar cells, only a part of the solar spectrum can be used for electricity generation, as shown in Figure 3. Only the part of the solar spectrum with more energy than the bandgap can contribute to the electrical output. However, since the bandgap also determines the output voltage of the solar cell, a trade-off exists in which the bandgap should be neither too low to produce a useful voltage, nor to high to take up a sufficient amount of photons. Photons that have an energy lower than the bandgap, may be absorbed to some extent in the cell but do not contribute to the generation of electricity. At the other hand, photons that have an energy higher than the bandgap are efficienctly absorbed in the cell, but only the part equal to the bandgap energy can be converted to electricity, while the excess energy is converted to heat by fast thermalisation in the lattice. Finally, part of the energy useful for electricity generation is lost due to recombination losses and ohmic losses. In Figure 3, the areas indicated as "not effective"and "wasted" both contribute to the heat generation in the cell. This heat production is undesirable in normal PV cells, since an increase in temperature reduces the electrical cell performance. However, in PVT applications one would prefer to minimize all reflection losses and retain all solar energy available.

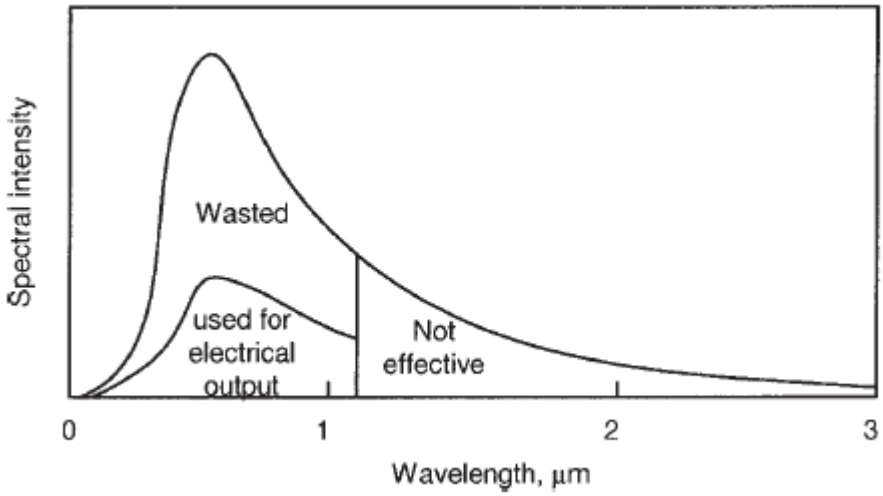

Figure 3: The effect of the spectrum on electrical efficiency of a solar cell.

In an ideal PVT configuration, all reflection losses would be minimized. In practice this means that the reflection at the front side of the cell should be minimized to optimize the high-energy absorption (above the bandgap). The absorption of low-energy light (below the bandgap) is much weaker and therefore an effort should be made to maximize the path length traveled by the light in the cell, and thereby the chance that the light will be absorbed. Since silicon has a high index of refraction compared to EVA, the escape cone from the silicon is small and internal reflection can be realized easily by means of diffusive reflection at the rear or texture.
In the following paragraphs, a summary is presented of the work carried out on the characterisation and numerical simulation of the absorption of solar cells at the EUT, as described in depth in the report 'PVT combi panels with various solar cell technologies', TUE-WET report 2006.24.

2.2 Experimental methods

By means of reflecting sphere measurements, the spectrally resolved reflection and transmission of polished wafers, textured wafers, textured wafers with antireflective coating, with or without emitter and with or without back contact were measured to be able to see the effect of each processing step in the production of a silicon solar cell. A summary is presented in Table 1.

Number	Front interface	Doped	Back interface	Spectral weighted absorption factor (A)
1	polished		sawn	0.52
2	polished		polished + Ni	0.64
3	Texture T1		polished	0.69
4	Texture T1 + ARC	P	polished	0.82
5	Texture T1 + ARC	P	polished + ARC	0.83
6	Texture T1 + ARC	P	polished + Al evaporation	0.89
7	Texture T1		sawn	0.64
8	Texture T1	P	sawn	0.71
9	Texture T1 + ARC	P	sawn	0.86
10	Texture T1 + ARC	P	Al silk screen printing + alloy	0.90
11	Texture T1 + ARC	P	sawn + Al evaporation	0.90
12	Texture T1 + ARC	P	sawn + Ni evaporation	0.91
13	Texture T1 + ARC	P	sawn + Cr evaporation	0.93
14	Texture T1 + ARC	P	sawn	0.85

Table 1: Crystalline silicon test structures and measured absorption factors.

From these results, it can already be observed that the absorption factor is increased by adding the anti-reflection coating (ARC), the doping, the texture and the rear contact. Although this table only shows the spectrally weighted absorption factor, the absorption was measured as a function of wavelength and the results were used to validate the numerical model, as described below.

2.3 Numerical model and validation

A numerical model was built, based on the net radiation method. This model incorporates both direct and diffuse reflection by means of reflection and transmission matrices at each interface layer in the PV, in which the reflection and transmission are presented as a function of ray angle. In addition, a ray tracing model was developed to determine the reflection and transmission matrices at textured interfaces. The model was then validated by comparing the model results to the experimental results described above. This resulted in the values presented in Table 2. A very good correspondence between model and experiments is clearly shown. Also the spectral measurements showed a good match with the simulations.

Description	A_{exp} (%)	A_{num} (%)
bare polished wafer	48±1	48
+ standard acid etch texture	64±1	64
+ phosphorous emitter	71±1	70
+ AR coating	86±1	83
+ aluminium back contact + BSF	90±1	88

Table 2: The experimental and numerical absorption factors for several unencapsulated solar cell test structures (A_{exp} corresponds to the data in Table 1).

2.4 Absorption in c-Si cells

By means of the model, the absorption of a large amount of configurations can now be calculated. The following figures show the spectrally resolved results of a number of c-Si configurations. Figure 4 shows the absorption of a planar solar cell (without texture or diffusive reflection), with encapsulation, antireflective coating and back contact. Clearly the effect of the bandgap is visible; almost all radiation above the bandgap is absorbed in the silicon, while only radiation below the bandgap is able to penetrate towards the back contact, where it is either absorbed or reflected. Note also the large effect of the free carrier absorption of low-energy irradiance in the emitter.

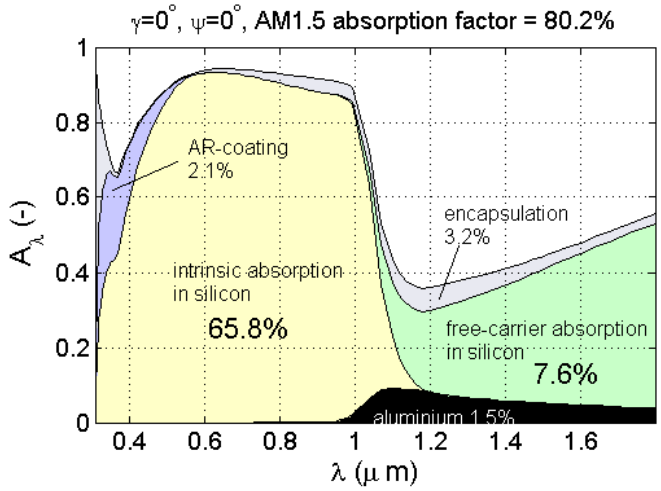

Figure 4: Simulation result for the spectral absorption factor of an encapsulated crystalline silicon solar cell with a planar structure and an aluminium back contact

In Figure 5 the effect is shown of a diffusely reflecting back contact; no changes occur in the high-energy part of the spectrum, but in the low-energy part now substantial diffuse reflection takes place at the rear of the cell, leading to full internal reflection of a large part of this light at the silicon –air interface where otherwise this light would simply have escaped to the ambient. Sine the pathlength of this light in the silicon is now substantially increased, the effect of free carrier absorption in the emitter also becomes much more prominent, increasing the total absorption to 85.6%.

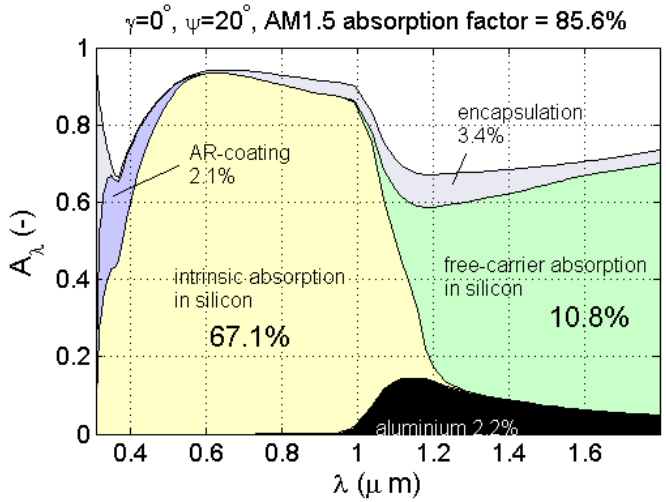

Figure 5: Simulation result for the spectral absorption factor of an encapsulated crystalline silicon solar cell with a planar structure and a diffusively reflecting aluminium back contact.

Finally, in Figure 6 the effect of texturisation is indicated. A texture on the surface has basically two effects; one is to promote internal reflection, much like a diffusely reflecting rear contact, and the other is to reduce reflection when the light first enters the cell. Therefore, one can see that now also the absorp-

tion in the high energy part of the spectrum is further enhanced, increasing the total absorption to over 90%.

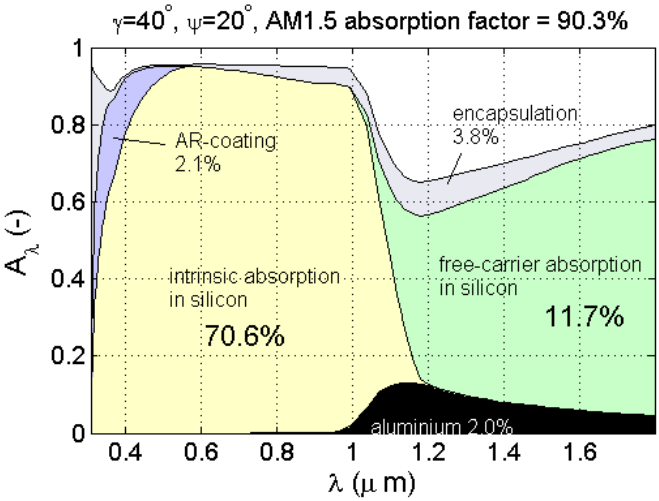

Figure 6: Simulation result for the spectral absorption factor of an encapsulated crystalline silicon solar cell with a textured front surface and a diffusively reflecting back contact.

One can conclude here that already for plane cells, the absorption of c-Si cells is a quite good 80-85% (depending on the diffusiveness of the back contact). However, if optimised textured cells are used, a further increase in absorption to over 90% is possible. These textured cells are already a standard product (since the texturisation is also directly beneficial to the electricity generation of the cell by its improved incoupling of high-energy photons), and for PVT applications therefore it is strongly recommended to use textured cells.

2.5 Absorption in thin film cells

A number of PV technologies exist in which not crystalline silicon cells are used, but much thinner 'film cells', such as amorphous silicon cells or CIS (Copper-Indium-diSelenide); while c-Si cells are typically 300 micron thick, thin film cells have a thickness of about 300 nm, so three orders of magnitude thinner. These cells can be made very thin because they have a much better absorption than c-Si (which has an indirect bandgap), as shown clearly in Figure 7b. Note also that a-Si has a large bandgap, which implies that the electrical energy produced has a higher voltage (but lower current) than for c-Si, while for CIS the opposite is the case. The cells have a TCO (transparent conductive oxide) layer, that functions both as an anti-reflective coating and as a means to transport the generated current towards the electrical contacts. These TCO layers are doped to obtain the required high conductivity, so free carrier absorption will now also play a role in the TCO.

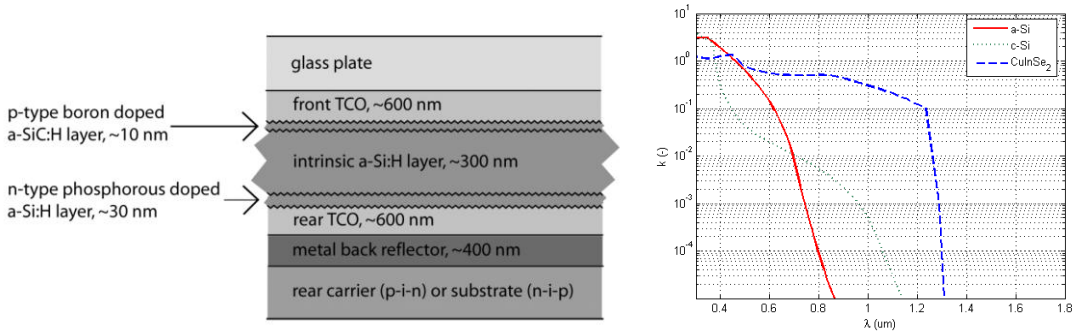

Figure 7 (a) Typical configuration for an amorphous silicon cell, (b) bandgap energy for amorphous silicon and CIS as compared to crystalline silicon.

Figure 8 shows the absorption of an a-Si cell. Since the bandgap is large, the absorption of the a-Si is only dominant over a small part of the spectrum, while the back contact has a much larger influence

than for c-Si. For a planar structure, the overall absorption is a meager 59%. This is increased if scattering is introduced, since this traps the light into the PV cell, thereby strongly increasing the absorption in the back contact and TCO, and improving the overall light absorption from 59% to 84%. In addition, also the absorption in the active a-Si is increased (from 29% to 34%), thereby improving the electrical performance of the cells. It should be concluded that the thermal performance of a-Si strongly depends on the effectiveness of the light trapping, which depends on the manufacturing method used.

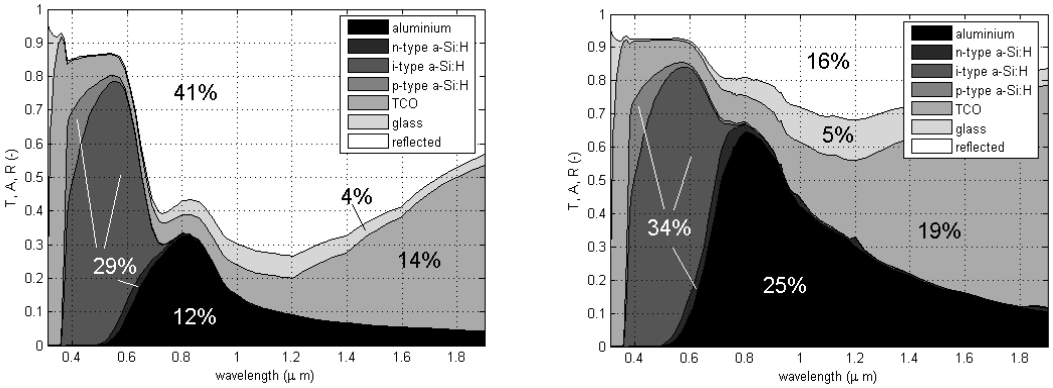

Figure 8: Absorption in amorphous silicon cells (a) all interfaces smooth, (b) scatter of irradiance by TCO and back contact.

In addition, many a-Si modules are produced with glass at both front and rear. Such modules can transmit part of the irradiance towards a secondary absorber underneath. The absorption of such a configuration is shown in Figure 9. It can be seen that only 11% of the light is reflected here as opposed to the 16% in the previous figure, while 31% is transmitted. If the transmitted light can efficiently be absorbed by a secondary absorber, this would also be an efficient configuration. However, this would require a transparent rear contact (like the back TCO in the figure) that is presently not standard.

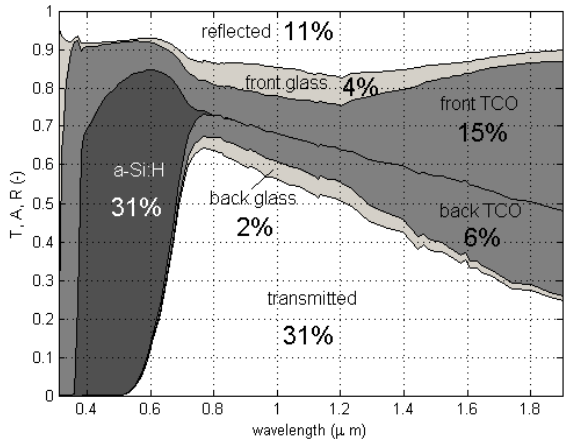

Figure 9: Absorption and transmission in glass-glass a-Si module (both front and back TCO scatter).

Finally, the absorption of a CIS module was calculated, as shown in Figure 10. Since the CIS has a small bandgap, a very large part of the spectrum is directly absorbed by the CIS and only a modest part of the irradiance reaches the back contact. If the back contact and the TCO layer are now again highly diffusive, low-energy absorption in the TCO and rear contact is important and an overall absorption of 91% can be reached. It can be expected, however, that the thermal performance of CIS depends much less on the effectiveness of the light trapping than the thermal performance of a-Si.

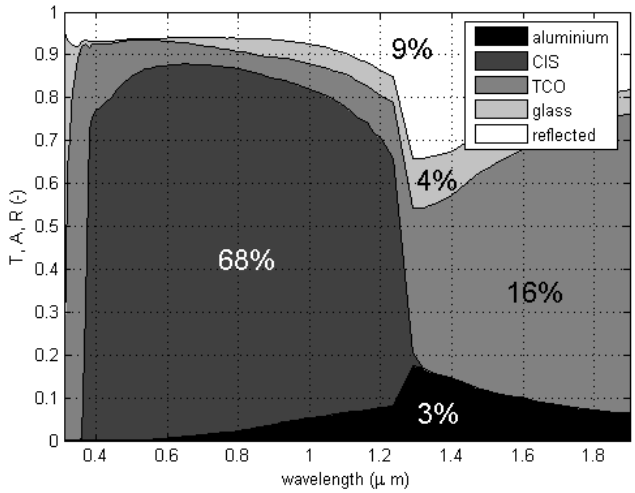

Figure 10: Absorption in CIS cell (assuming scattering of TCO and rear contact)

A summary of all thin film results is presented in Table 3.

description	front TCO scatter model	back contact scatter model	a-Si:H		CIS	
			A_{total} (-)	A_{semi} (-)	A_{total} (-)	A_{semi} (-)
no confinement	specular	specular	59%	29%	82%	64%
modest confinement	haze (δ_{rms}=45nm)	haze (δ_{rms}=45nm)	74%	33%	87%	67%
good confinement	haze (δ_{rms}=135nm)	phong (ψ=45°)	84%	34%	91%	68%

Table 3: Overview of thin film absorption results.

In addition to the work by Van Zolingen (2006) presented above, a calculation of the collector efficiency curves based on these absorption coefficients was later carried out by Zondag, as described in Appendix A.

2.6 Conclusions

It was found that planar (non-textured) c-Si cells have already a moderately good absorption of 80-85% (depending on the diffusiveness of the rear contact). This can be further increased to 90% if effective texturing is applied. For thin films, CIS can reach a very high absorption of 91%. For a-Si, the total absorption is lower and strongly depending on the effectiveness of the light trapping. Finally, glass-glass a-Si modules may successfully be combined with a secondary absorber, provided that these modules have a TCO rear contact that provides effective transmission of the light.
For the short term, it is recommended that for PVT mainly textured c-Si cells are used, since these have a very high absorption, a high electrical efficiency (increasing the primary energy savings of the PVT) and are probably the most reliable technique given the harsh conditions in a PVT collector. However, if thin film options are considered, CIS seems a promising alternative with a potentially very high absorption.

3. CIS PVT modules

3.1 Choice for CIS as thin film PVT material

Crystalline Si is presently the main PV material in both PV and PVT, and has many advantages such as its reliability and high conversion efficiency. However, thin film cells are much thinner, thereby requiring less material and production energy, which causes thin film cells to be seen as a promise for the future. A number of different types of thin film material exist, such as aSi, CIS and CdTe. From the optical results presented in chapter 2, it seems that CIS has the best solar absorption. It was also seen that the good performance of CIS was related to its small bandgap, thereby reducing the reflection losses. Table 4 shows the bandgap of a number of PV materials. As can be seen, CIS has the smallest bandgap of all presently used materials, thereby providing the highest absorption. However, it should be realized that CIS is now largely displaced by CIGS, which has a higher electrical efficiency due to its slightly higher bandgap, resulting however also in a slightly lower absorption. Note that amorphous silicon, CdTe and CuInS2 cells (also called CIS, produced by the company Sulfurcell) have a large bandgap and therefore are expected to have higher reflective losses.

Cell type	Bandgap (eV)
Copper-Indium-diSelenide	1.04
Copper-(indium,Gallium)-diSelenide	1.11
Crystalline Silicon	1.1
Cadmium Telluride	1.45
Copper-Indium-diSulfide	1.57
Amorphous Silicon	1.6-1.8 (depending on H content and substrate temperature)

Table 4: Bandgap energy for different cell types (data from Archer and Hill, 2001).

Since it has also a good electrical performance, it was chosen to focus in this chapter on the possibility of a CIS PVT collector. It should be stressed here that the present chapter is just an inventory of the theoretical possibility of such a concept, while practical realization is still a long way off.

3.2 Characteristics of CIS

Van Zolingen and Santbergen (2006) showed that CIS has a very good absorption factor compared to amorphous silicon PV technologies. Their results are displayed in the table below.

description	front TCO scatter model	back contact scatter model	a-Si:H		CIS	
			A_{total} (-)	A_{semi} (-)	A_{total} (-)	A_{semi} (-)
no confinement	specular	specular	59%	29%	82%	64%
modest confinement	haze (δ_{rms}=45nm)	haze (δ_{rms}=45nm)	74%	33%	87%	67%
good confinement	haze (δ_{rms}=135nm)	phong (ψ=45°)	84%	34%	91%	68%

Table 4.1: The absorption factor of the total configuration A_{tot} and the semiconductor layer A_{semi} for an a-Si:H cell and a CIS cell for different degrees of optical confinement.

Table 5: Solar absorption by aSi and CIS (Van Zolingen, 2006)

The spectral composition of the absorption is further shown in Figure 11. These calculations show that 91% (see Figure 11a), or for very good confinement even 94% (see Figure 11b) of the light is absorbed in the sandwich, of which 68-71% in the CIS and 16-17% in the TCO layer. The free carrier absorption in the TCO gives a very significant contribution.

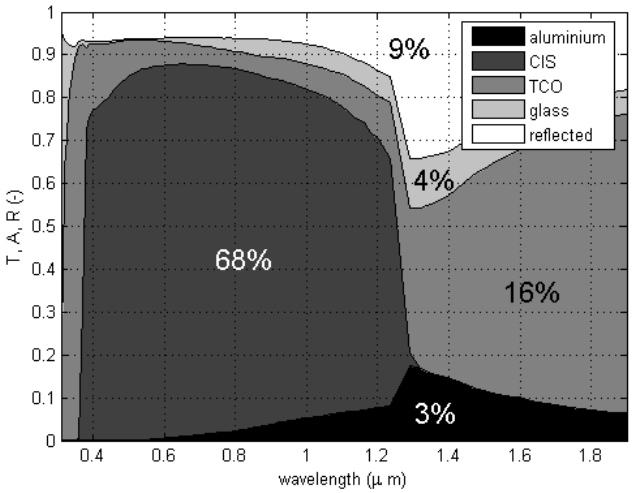

Figure 11: Spectral composition of the solar absorption of CIS (Van Zolingen, 2006).

A warning is given that the results from Santbergen only take into account Cu-In-Se_2, without addition of Ga. Since the addition of Ga slightly increases the bandgap, it can be expected that also reflection losses will slightly increase. Since in commercial modules Ga is generally added to CIS (De Moor, pers comm.), the calculated values give a slight overestimate of the absorption that will be found in commercial CIS modules.

3.3 Manufacturing procedure of CIS

3.3.1 Glass-glass modules

Rau and Schock (Archer & Hill, 2001) indicate that a CIS module consists of a soda-lime glass, on which an Mo back contact layer is deposited, then the Cu(In,Ga)Se_2 layer, then a CdS layer (by Chemical batch deposition) and finally an undoped ZnO layer (sputter deposition) and finally a heavily doped ZnO layer. They indicate the following improvements that occurred over the years

- Na diffusion from the glass through the Mo into the active layer strongly improves the efficiency and reliability of the cells. To promote this, before the active layer is deposited, Na-containing precursors may be deposited such as NaF, Na_2Se or Na_2S, which also allows other substrates than soda-lime glass. Initially, blocking layers such as SiN_x, SiO_2 or Cr were deposited between the glass and the Mo to prevent diffusion of Na from the glass, but this practice was ended when the effect of this diffusion was found to be actually beneficial.
- The addition of Cu_xSe improves the film quality
- Partial replacement of In by Ga (20%-30%) increases the bandgap which gives a better match to the solar spectrum, and also improves the electronic quality
- Initially a CdS top electrode was used that was deposited by PVD; this was changed to CdS deposited by chemical batch deposition combined with a highly conductive ZnO window layer. The CdS layer has many benefits; among others it gives a full coverage of the rough CIS surface and protects it from damage by the ZnO deposition process, while removing Se and the natural oxide.

The sequence mentioned here corresponds to other literature data, e.g. Figure 12 on the Siemens process.

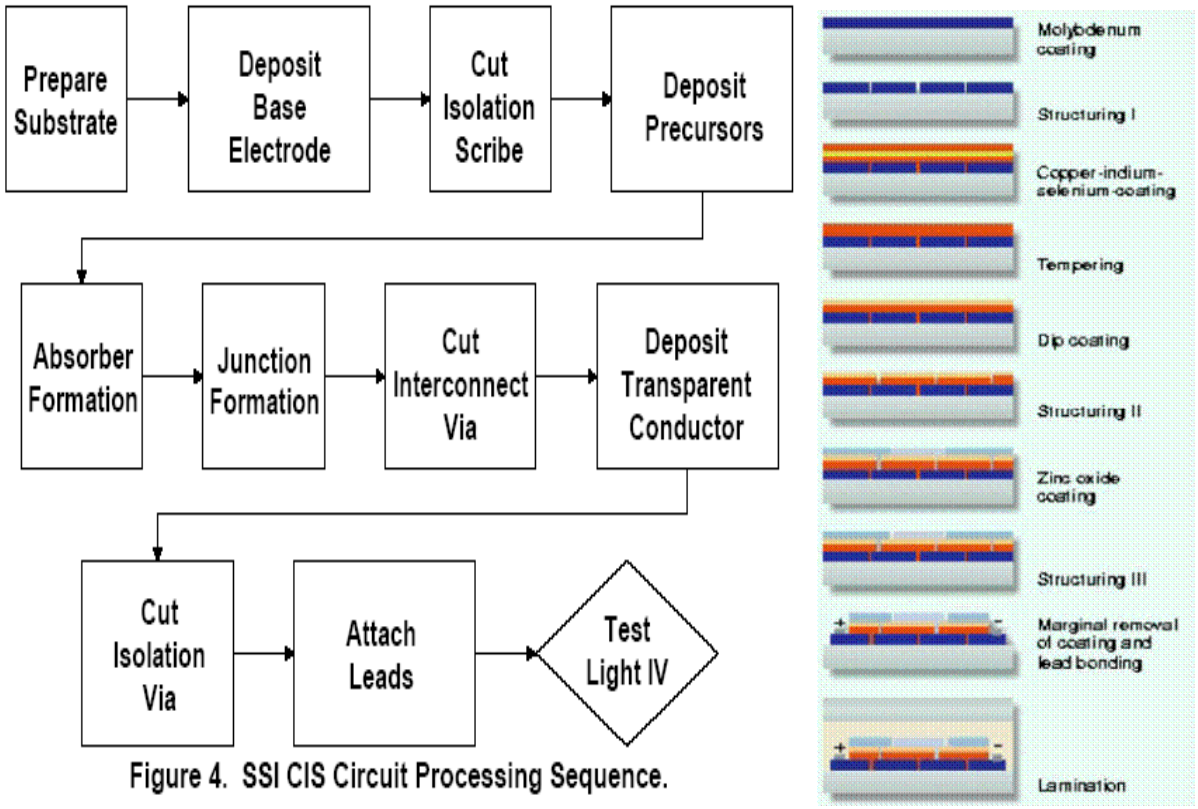

Figure 12: CIS processing sequence Siemens process with Copper-Indium Diselenide (Tarrant, 2004).

Information on layer composition and thickness is available from various sources. Figure 13 and Figure 14 show information on the Siemens layout, whereas Figure 15 gives information from Dhere (2006). It can be seen that the results are largely the same. The main difference is the variation in the ZnO layer, varying from 400 to 1500 nm. All modules have a very thin CdS buffer layer (20-50 nm), and a thick active layer of Cu(In,Ga)Se2 of 800-2500 nm, with a Mo rear contact of 350-900 nm, deposited on the rear glass.

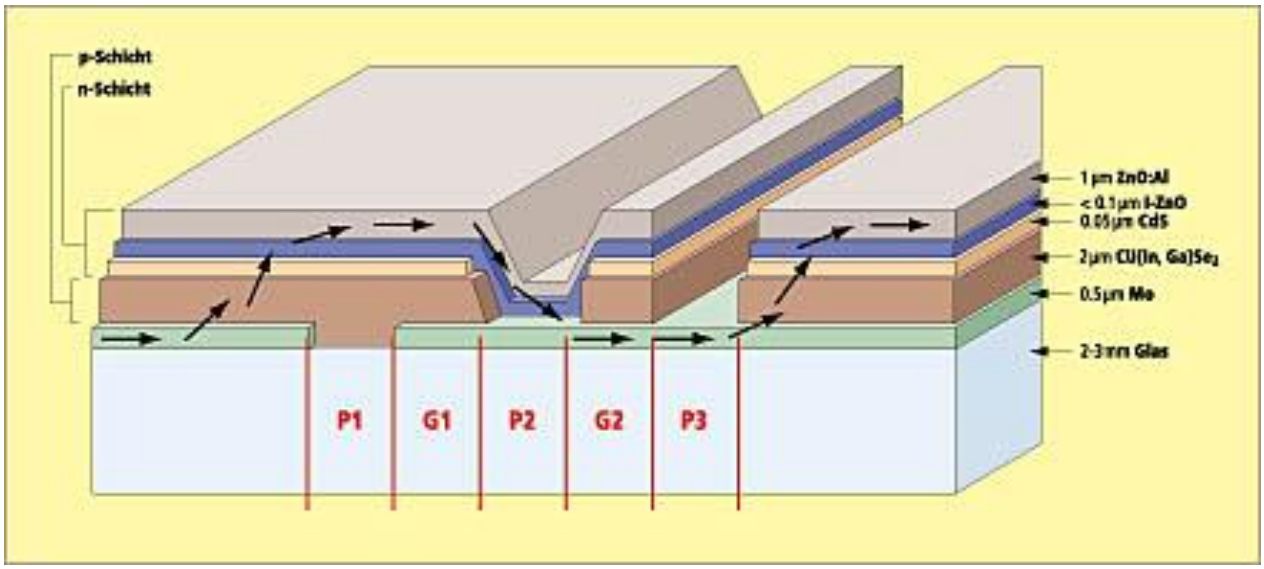

Figure 13: Siemens CIS cell layout (Siemens documentation).

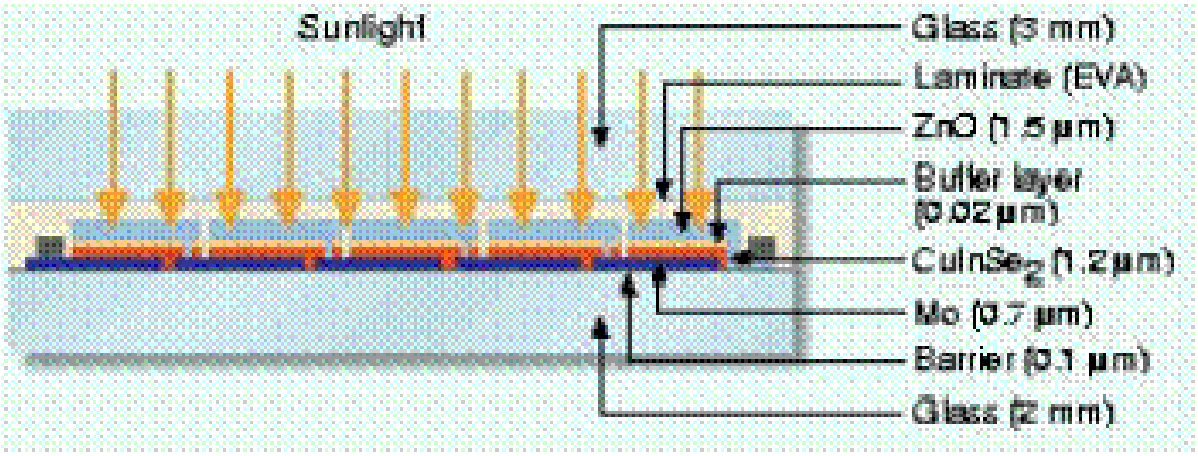

Figure 14: CIS processing sequence (Siemens documentation)

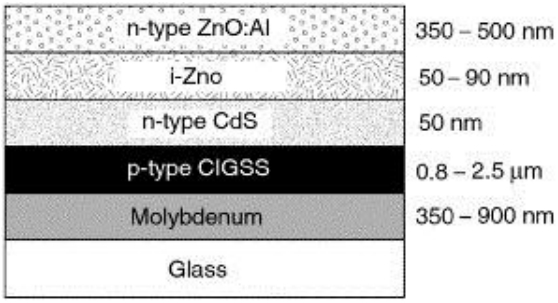

Figure 15: CIS layout as given by Dhere (2006)

Further information on commercially available CIS modules is presented in Appendix B.

The most important conclusion from this is that the active CIS layer is deposited on the rear glass. This is different from a-Si modules, for which also deposition at the top glazing is standard (Archer & Hill, 2001, page 221-225). If the deposition is at the top glass, like a-Si, it is possible to laminate the thin-film-glazing directly onto a copper absorber (replace rear glazing by copper absorber). However, since the CIS is deposited on the rear glazing, it is necessary to connect the rear glazing to the copper absorber and still use a top glazing to protect the CIS from moisture etc. The differences in thermal expansion between the rear glass and the copper will require a thick and elastic connecting layer to deal with the corresponding stresses. Compared to c-Si PVT this system contains additional layers of glass and glue (or EVA) that cause extra processing steps, cost extra material and cause additional thermal resistance. In particular, the thermal stresses between the metallic absorber and the glazing will require thick elastic layers of glue or EVA that increases the thermal resistance and may also lead to a reduced lifetime of such modules. In addition, the additional glass increases the weight of the module. These issues make modules with CIS deposited on glass less suitable for PVT application.

3.3.2 Flexible CIS modules

Normally, CIS is deposited on glass, but also flexible substrates are under research. Several manufacturers have announced research into CIS on flexible substrates such as Würth together with ZSW and ISET, but it seems that at present only Global Solar presently has a market product

Global Solar seems the only company that presently has a flexible CIS market product (as also claimed on their website). Their website indicates that since 1996 Global Solar Energy has evolved into a major producer of thin-film photovoltaic Copper Indium Gallium DiSelenide (CIGS) solar cells and that GSE is now the leading manufacturer of CIGS thin-film solar on a flexible substrate. This seems to be based on their market introduction of the PowerFlex modules in 2008, announced as a breakthrough. Unfortunately, little information could be found on their production technology.

Figure 16: Flexible CIGS modules from Global Solar (a) prototype, (b) & (c) commercial PowerFlex modules

The University of Delaware's IEC (Institute of Energy Conversion) has started developing flexible CIGS in 1995 as part of a consortium through a multi-year program funded by the Defense Advanced Research Projects Agency, the primary research and development arm of the Department of Defense. It seems likely that this is connected to the development at Global Solar, since Global Solar and IEC have common patents on this subject (see www.freepatentsonline.com/6372538.html), but little information could be found on this. In an interview of 2007 with IEC, the following was indicated:

> Flexible solar cells 10 inches wide and up to 50 feet in length are being produced at the University of Delaware. This also provides for lightweight and flexible solar cell panels that could find interest in the space, military and recreational markets. For standard applications, the solar cells can also be encapsulated into a more traditional rigid structure. By being flexible, the solar cells can conform to different surfaces. The solar cell sheets are created by depositing copper-indium-gallium-diselinide, which the IEC scientists call CIGS, on a 10-inch wide polymer web, which is then processed into the flexible solar cells. CIGS solar cells are currently the only thin-film technology that has achieved efficiencies comparable to silicon solar cells, presently the standard of the industry. IEC does not have the facilities to process the web into solar cell modules but is working with other organizations to commercialize the technology. However, IEC has evaluated the quality of CIGS on the molybdenum-coated web by characterizing the uniformity of the film. Researchers found that average solar cell conversion efficiencies of 10 percent were achieved. Thin-film CIGS-based solar cells have a multi-layer structure stacked on a substrate, in this case a high-temperature polyimide substrate that is coated with molybdenum, CIGS, cadmium sulfide, zinc oxide and indium tin oxide. All the component films of this structure can easily be processed on flexible substrates. In fact, CIGS is the most difficult layer because of high substrate temperature and thermal deposition from four different elemental sources, since this process results in the best performing solar cells. A major breakthrough occurred in 2003 and since then researchers have been improving the quality and throughput. Presently IEC is at a stage where they can make flexible CIGS of 10-inches in width and 50 feet in length, and which demonstrates efficiencies around 10 percent. www.udel.edu/PR/UDaily/2007/mar/solar032307.html

In a publication from ZSW and Würth (Powalla, 2005) the following overview was given:

> The most promising flexible substrates are currently polyimide and titanium. When using polyimide substrates, the process temperatures must remain under 400°C, less than ideal for high-quality absorber deposition. Various techniques have been explored for introducing sodium into the absorber which normally diffuses from the glass substrate during the high-temperature CIS deposition process. Using the Na precursor method, cells up to 11.2 % (0.5 cm2) and monolithically integrated modules up to 7.5 % on 10 x 10 cm2 and 5.2 % on 20 x 30 cm2 could be produced. Photolithography techniques were applied for the module patterning steps.
> Depositing modules on a metallic, electrically conducting substrate complicates their monolithic integration: they require an insulating film between the substrate and the device layers. The results for monolithically integrated modules on Ti foil are still relatively modest. Using a SiOx barrier film results of 6.8 % on 7 x 8 cm2 and 3.8 % on 20 x 30 cm2 have been achieved. Best overall results so far are achieved on large single cells which can be connected with a shingling technique. Using titanium foil, an average efficiency of 11.4 % (AM 1.5) was already achieved in the small-series production of large single cells, with a best efficiency of 13.8 % (Voc: 647 mV, FF: 72.3 %, jsc: 29.5 mA/cm2).

An example of the flexible CIS modules developed by ZSW is shown in Figure 17

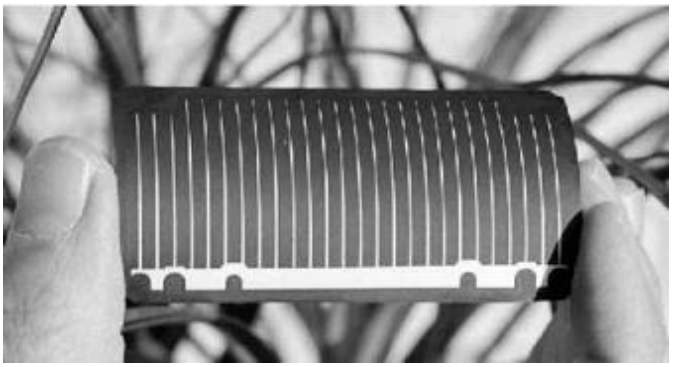

Figure 17: ZSW flexible CIS cell 4 x 8 cm2 CIS solar cell on 25 µm Ti foil (Powalla, 2005).

Also, CIS on flexible substrate is developed for space applications by the R&D company ISET. In 2005 ISET was granted a contract to develop thin film CIGS photovoltaics on flexible ceramic substrates for application on High Altitude Airships (HAA). Kapur, the president of ISET, indicated the following in 2003 (Kapur, 2003):

In the past, ISET fabricated CIS/CIGS solar cells on Mo foil and polymeric 'Kapton' substrates. In these efforts absorber layers of CIS/CIGS were deposited using a 'Two Step Process' employing vacuum deposition of metallic precursors followed by their selenization [4,5] with promising results. However, recently, ISET successfully applied its non-vacuum process for fabricating CIGS solar cells on flexible metallic foil substrates [6]. Table 1 shows the weight contribution of a variety of flexible substrates of thickness 0.001" to the CIGS circuit. Using the non vacuum process, we have fabricated CIGS solar cells on Mo and Ti foils. At ISET we have not yet worked on stainless steel foils. To achieve the highest power density, CIGS solar cells should be fabricated on the lightest polymeric substrate such as 'Kapton' and 'Upilex'. These flexible substrates, with the exception of the Mo foil, are metallized by depositing a thin layer (0.4µm) of Mo by sputtering. The coefficients of expansion (CTE) of these substrates vary over a wide range. A CTE mismatch between the metallized substrate and the CIGS layer deposited on it can cause adhesion problems between the CIGS layer and the substrate. Therefore for every substrate the cell fabrication process has to be optimized to promote adhesion between the metallized substrate and CIGS layer deposited on it.

Table I. Power Density vs. Substrates

	CTE (X 10^6/°C)	Density g/cm^2	Weight£ g/m^2	Power Density* W/Kg
CIGS cell				
CIGS cell (with contacts & transparent cover layer)	7-9		33-40	
Flexible Substrates				
Molybdenum	4.8	10.2	259	455-466
Stainless Steel	12-17	7.9	205	555-574
Titanium	8.6	4.5	118	861-901
Kapton	20	1.42	40	1700-1863
Polyimide (Upilex-S)	12	1.47	41	1679-1838

* Assuming a 1 mil (25.4 µm) foil, 10% AM0 cell, and AM0 incident power = 1360 W/m^2. £ For Power Density calculations all substrates except Mo foil assume a 0.4µm thick Mo coating on one side of the substrate. Each 0.4µm Mo coating adds 4.1 g/m^2 to substrate weight. CTE = Coefficient of Thermal Expansion.

It must be concluded that although flexible CIGS is becoming available, it is far from a well established product with presently only one manufacturer and still has to prove itself in practice. This is an insufficient basis for PVT development along this line. For the short term, only glass-glass CIS modules will be available in which the CIS is attached to the rear glazing, while the top glazing is laminated to the module by means of EVA. For the future one may think of a flexile CIS module on a metallic substrate with small thermal expansion (such as stainless steel) that could at the same time function as a thermal absorber, but this will require a broader manufacturer base than is presently the case.

3.4 Recommendations for further testing

It is recommended to do optical characterisation of CIS PV modules to establish the actual absorption of these modules. If this is satisfactory, it is recommended to do high temperature cycling testing on a CIS module. Since it may be necessary to use commercially available CIS glass-glass modules that are already laminated, it is recommended to test a low-temperature method (flexible glue or silicones) for the connection of the CIS module to the copper absorber, because heating a laminated module anew in a laminator will certainly lead to degradation of the module. Also here, cycling experiments with this system in a climate chamber should be carried out and the thermal resistance should be measured.
For the future, it could be interesting to test the application of flexible CIS modules, but since these modules are still under development and their reliability is not sufficiently clear, this is presently not an option.

4. Reduced radiative and reflective loss from PVT glazings

4.1 Introduction

This chapter is a short summary of the report by Van Zolingen (2008), that was written as part of the WAELS project. For further information, the reader is referred to this report.

4.2 Effect of anti-reflective coatings for PVT glazings

The companies Flabeg and Sunarc started the production of special antireflective low-iron glass for solar applications. Typically, for these glazings solar transmissions of 95-96% are claimed by Sunarc, while Flabeg claims solar transmission up to 97%. As seen in Figure 18, these glazings have a substantially higher transmission in the solar spectrum than conventional glazing. Increasingly, 1-side coated glazings are used by PV manufacturers for PV modules.

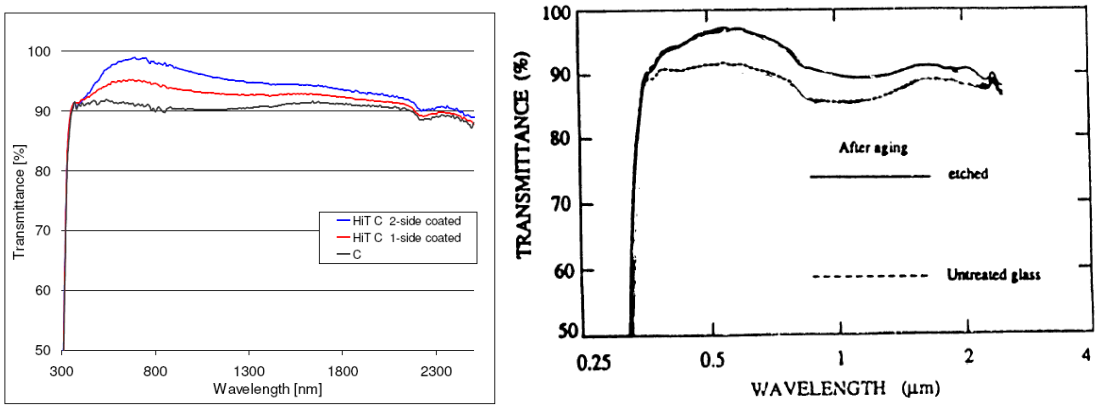

Figure 18: Transmission spectrum of (a) Flabeg Centrosol Clear and Centrosol High-Transmission Clear glass (product brochure), (b) Sunarc glass (test report Uppsala University and Alvkarleby laboratory).

If such a glazing would be applied in a PVT module, the reflection losses would be reduced, by which both the PV efficiency and the thermal efficiency would increase. These coatings could be applied on both the PV glazing and the glass collector cover, as shown in Table 6a. The resulting absorption factors and efficiencies are shown in Table 6b.

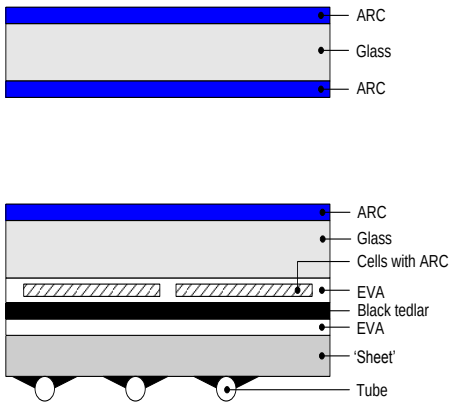

	No cover		Cover	Cover with ARC on both sides
	No ARC on laminate	ARC on laminate	No ARC on laminate	ARC on laminate
Active area electrical cell efficiency (%)	16.36	17.11	15.09	16.51
Total area electrical cell efficiency (%)	15.62	16.34	14.41	15.77
Total area electrical collector efficiency (%)	14.06	14.71	12.97	14.19
Active area cell absorption factor (%)	91.12	93.80	83.17	90.42
Total area collector absorption factor (%)	88.58	91.16	80.95	87.91

Table 6: (a) PVT absorption factor and electrical efficiency for various configurations with antireflective glass, (b) collector configuration with coatings indicated

In addition to the work by Van Zolingen (2008) presented above, in order to assess also the potential for a double cover with antireflective glazing, some extra calculations were later carried out by Zondag, as described in Appendix A.

4.3 Low emissivity coatings

4.3.1 Theoretical background

Low emissivity coatings are frequently used in glazings to reduce the radiative losses. These coatings can be made in two ways; either with very thin metal layers, or with doped semiconductor layers. Essential in these two materials is the presence of free electrons, that give these materials their reflective properties in the infrared. Unfortunately, these coatings also have some reflection and absorption in the solar part of the spectrum. Particularly in metallic low emissivity coatings, the solar transmission is significantly reduced. Therefore, the present report will focus on doped semiconductor coatings, and more particularly on fluor doped tin oxide SnO_2:F that is mostly used as low emissivity coating for window glazings. Other potentially interesting coatings are ITO, which is mostly used in flat panel displays and ZnO:Al, that has been used more for electronic applications, but since these coatings have not yet been applied as low-emissivity coating (Santbergen, 2008), these are not the main focus here.

The reflection properties originating from free carriers in metals and (doped) semiconductors can be described by the Drude model, as described by Haitjema (1991). From this model, two important parameters can be deduced;

- the plasma wavelength that describes where the reflectance changes from highly reflective to low reflective. For increasing the reflective range to higher energy levels, one can increase the number of electrons.

  $$\lambda_P = \frac{2\pi c}{\omega_P}, \text{ with } \omega_P = \left(\frac{ne^2}{\varepsilon_0 \varepsilon_\infty m_{eff}} \right)^{1/2}$$

- the ratio between the attenuation wavelength and the plasma wavelength, that describes how fast (selective) this transition is. For a good selectivity, this ratio needs to be as high as possible; which can be done by increasing the free carrier concentration and the electron mobility.

  $$\frac{\lambda_\gamma}{\lambda_P} = \mu \sqrt{\frac{m_{eff} n}{\varepsilon_0 \varepsilon_\infty}}$$

Both effects are seen in Figure 19 for a typical low-emission coating. Furthermore, this figure also shows the oscillations occurring at short wavelengths for such a TCO layer, since the wavelength of the light is of the same order as the thickness of the TCO, resulting in interferences. In Figure 20, measured transmission and reflection spectra are presented for different coatings.

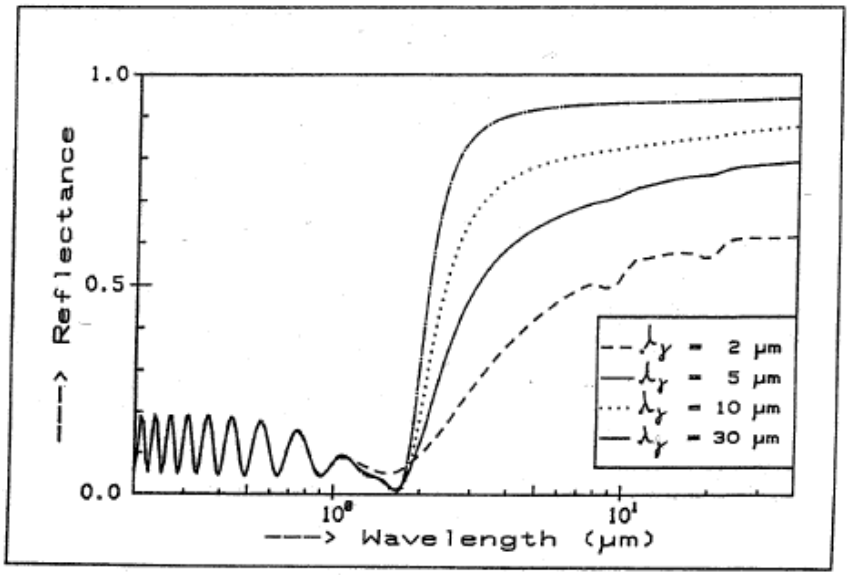

Figure 19: Reflection of a low-emission coating.

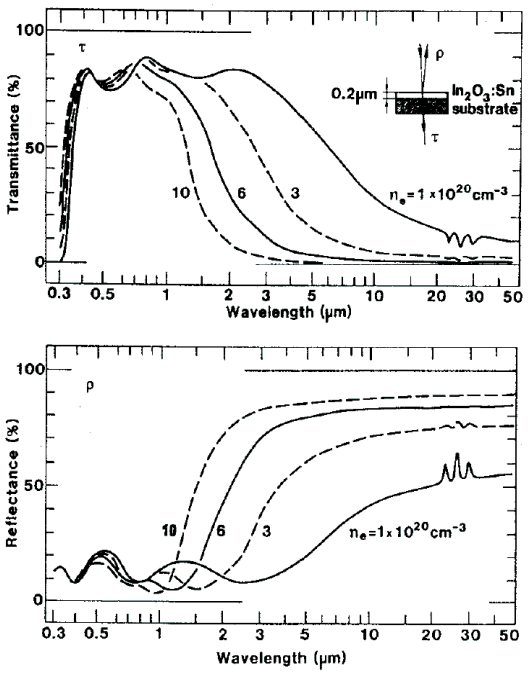

Figure 2.18 Spectral normal transmittance and reflectance computed from a quantitative model for the optical properties of In_2O_3:Sn. The values of electron densities (n_e) and coating thicknesses used are as shown.

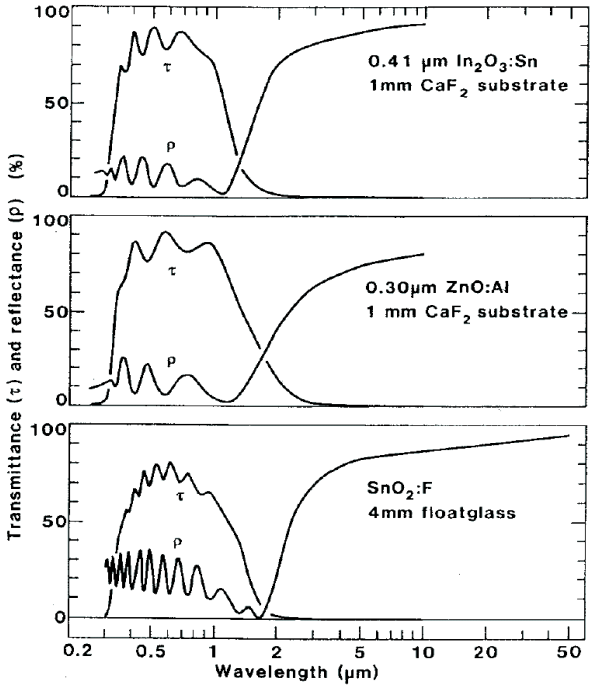

Figure 2.19 Spectral transmittance and reflectance measured for In_2O_3:Sn on 1 mm CaF_2, ZnO:Al on 1 mm CaF_2, and SnO_2:F on 4 mm float glass. Coating thicknesses are given.

Figure 20: (a) Effect of electron density in ITO coating (Gordon, 2001), (b) Spectra of different coatings (Gordon, 2001).

For a SnO_2 coating as a function of coating thickness, Figure 21 shows the emissivity and transmission, derived by Van Zolingen (2008) from results of Haitjema (1989).

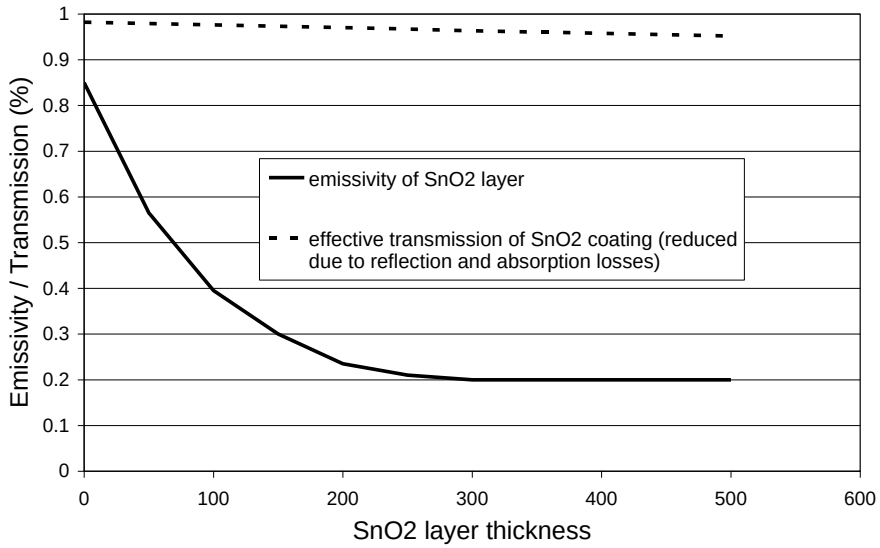

Figure 21: Emissivity and transmission of a SnO_2 coating, as a function of coating thickness (Van Zolingen, 2008).

4.3.2 Effect of low-emissivity coatings for PVT glazings

In Table 7, the effect of a 300 nm thick low-emissivity coating on the PVT absorption factor is indicated. The low-e coating clearly reduces the electrical performance; with 7.5% relative in the case without antireflective coating, and with 3.7% in the case with antireflective coating. The effect on the absorption factor is less, because the part of the irradiance that is absorbed in the antireflective coating reduces the electrical efficiency, but not the absorption factor.

	Without ARC	With ARC	With low-e coating	With low-e coating with ARC on top	With low-e coating sandwiched between 2 ARC's
Total area electrical collector efficiency at STC (%)	13.74	14.19	12.72	13.67	13.79
Total area collector absorption factor (%)	85.43	87.91	80.92	86.66	87.30

Table 7: The application of antireflective coatings and low-emissivity coatings in PVT modules. All configurations have a cover with antireflective coatings on both sides.

4.4 Effect of coatings on system efficiency

It has been assessed in the previous paragraphs how the antireflective coatings and the low-emissivity coating affect the absorption, the electrical efficiency and the emissivity, but not yet what this means for the annual performance of a PVT system. Calculations for the annual performance of a Solar domestic hot water system are shown in Table 8.

	Cover without ARC		Cover with ARC		
	No low-e coating		No low-e coating		Low-e coating
	No ARC on laminate	ARC on laminate	No ARC on laminate	ARC on laminate	Low-e coating with ARC on top
Total area electrical collector efficiency at STC (%)	12.97	13.36	13.74	14.19	13.67
Total area collector absorption factor 0(%	80.95	82.95	85.43	87.91	86.66
SDHW system					
Annual electrical efficiency (%)	9.96	10.22	10.46	10.74	9.75
Annual thermal efficiency (%)	24.3	24.7	25.1	25.5	28.0
Combined SDHW and RH system					
Annual electrical efficiency (%)	9.84	10.09	10.33	10.61	9.71
Annual thermal efficiency (%)	14.0	14.3	14.7	15.1	17.7

Table 8: Effect of coatings on the annual thermal and electrical efficiencies on (a) a solar domestic hot water system and (b) a combi system (tap water and space heating).

From these results, it is clear that the low-emissivity coating has a strong positive effect on the thermal performance, but also a significant negative effect on the electrical performance, due to both increased reflection losses and increased collector temperature (which negatively influences the PV efficiency). Note here that the reduced radiative losses will also strongly increase the stagnation temperature of the PVT.

In order to further investigate the optimisation of the low emissivity coating, the thickness was varied. The results are shown in Figure 22. 'G' refers to the case without low-emissivity coating. Note that 'G' performs better than a zero thickness coating, since such a coating still has reflection losses.

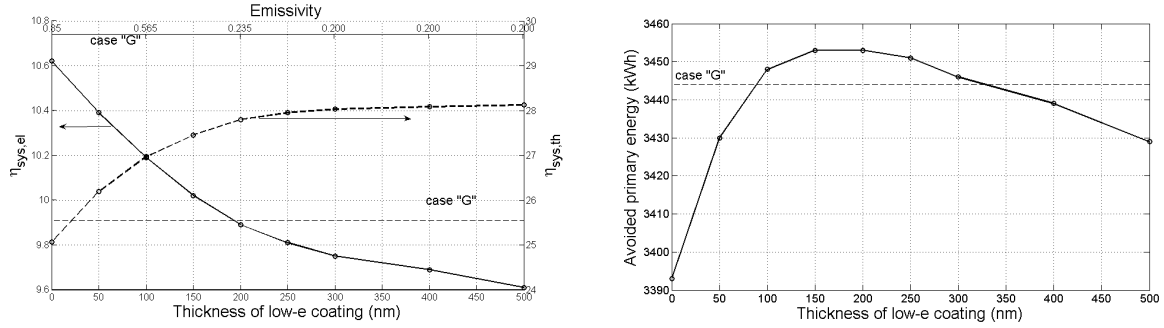

Figure 22: Effect of thickness of low-emissivity coating on annual PVT efficiency. 'G' refers to the case without low-emissivity coating.

In Figure 22b, the primary savings are indicated. It is clear that only a small positive gain can be obtained from the low-emissivity coating, which is highest for a coating of about 150 microns thickness, corresponding to an emissivity of 30% (see Figure 21).

4.5 Conclusions

The conclusions presented below are copied from the report by Van Zolingen (2008).

- The application of AR coatings in covered PVT collectors on both sides of the cover plate and on the encapsulant of the solar cells is favorable because it increases both the annual thermal efficiency (up to about 5% relative) and the annual electrical efficiency (up to 10% relative).

- By the use of an AR coating on both sides of the cover plate in a covered PVT collector, the practical minimum transmission loss of about 2.3% is reached.

- The electrical efficiency loss at STC introduced by a low-e coating compared to an AR coating is about 4.8% if only an AR coating on top of the low-e coating is used and about 4.0% if the low-e coating is sandwiched between two AR coatings. This loss can be reduced to about 3% in the case that the low-e coating is sandwiched between two AR coatings if the internal absorption (in the visible and near infrared region) in the low-e coating is reduced to 1% relative.

- The introduction of a low-e coating will reduce the annual electrical efficiency, however, severely (up to 10%), making the application of a low-e coating less attractive, unless the annual thermal efficiency has priority over the annual electrical efficiency.

- From an avoided primary energy point of view there exists a trade-off between the annual electrical efficiency and the annual thermal efficiency in tuning the thickness of the low-e coating in a covered PVT collector.

- So far, the option of using only AR coatings, so without a low-e coating, seems to be the most attractive.

5. Unencapsulated cells in protective atmosphere

5.1 Concept

One important reason for the low thermal performance of PVT modules is the fact that such collectors do not have a low-emissivity absorber. Since radiative losses make up for a very substantial part of the total losses of a collector, it is important to reduce these losses. Basically, two methods exist:

- Apply a low-emissivity coating to the module glazing or to the inner side of the top glazing
- Leave the PV material unencapsulated. Typically, the active PV material (both the heavily doped p-type top surface of cSi cells and the TCO coatings on thin film PV) has a low emissivity top surface. This is due to the high electron mobility, which is also required to have sufficient electrical conductivity.

The first method is treated in chapter 4, while the second method will be focused upon here. The present chapter focuses on the theoretical calculation of the resulting module thermal efficiency when unencapsulated cells would be applied.

Typical TCO's used for thin film are In_2O_3:Sn (=ITO= In_2O_3 + 0.2-2% Sn), SnO_2, ZnO:Al and Cd_2SnO_4; which are used on all PV-types with a high sheet resistance (a-Si:H, CIS, CdTe) (Archer & Hill, 2001, p. 137). ITO and SnO2 are typically used on a-Si, ZnO on CIS and In_2O_3 with a SnO_2 buffer layer or Cd_2SnO_4 on CdTe. Although thin-films are interesting because of the low emissivity of the TCO's, they also have a number of disadvantages that make them less suitable for this application:

- CIS has a CdS bufferlaag (Archer & Hill, p. 301) and also CdTe contains Cadmium. Due to health care regulations, this cadmium should be well locked into the laminate. Therefore, these types of PV seem less suitable for unencapsulated application.
- a-Si with ITO coating could be a possible option, but a-Si is very sensitive to moisture and also its electrical and thermal efficiency is rather low. Therefore it is not suitable for an advanced PVT module.
- Stability of the ZnO layer in humid environments is a major concern. Indium Tin Oxide (ITO) is superior in this respect (Archer & Hill, 2001, p. 301).

Finally, the availability of Indium may affect choices for thin-film PVT development. It seems that the worldwide amount of Indium is rapidly depleted as shown in Table 9. This is a point of attention both for CIS and for ITO coatings. However, due to increased efficiency of Indium extraction, indium can now be obtained from sources of lower concentration and as mining byproduct from a wider range of metals, making a larger volume economically available[a]. In addition, efforts are ongoing to replace indium by other materials. Therefore, it seems that Indium scarcity may be a point of attention but probably not a future bottleneck.

	Technology	WRLI in years Based on reserves	WRLI in years Based on Reserve base
Ag	x-Si	14	29
Cu	interconnection	31	61
In	CIGS	6	13
Sn	TCO	22	40
Te	CdTe	164	367
Ru	Dye sensitized	525	940
Pt	Dye sensitized	198	392

[a] The Indium Corporation gave the following information on the Indium supply at the PVSEC 2007: "For primarily economic reasons, indium was originally only extracted from zinc and lead concentrates containing at least 500 ppm indium (and coming from ores containing about 50 ppm of indium). Due to improvements in the extraction technology combined with the economics of higher prices; Indium is now recovered as a by-product of a wider range of base metals including tin, copper and other polymetallic deposits. Indium is also now being extracted and recovered from base metal concentrates containing as little as 100 ppm of indium." Phipps (2007).

Table 9: Depletion in World reserve life index (years). (From De Wild, 2007).

In the literature, very limited information can be found on unencapsulated PV for PVT applications. The main research that could be found was carried out by Platz (1997) and Affolter (2000), whose emissivity measurement results are shown in Table 10. However, they present measured emissivities without mentioning the thickness of the TCO layer, the dopant concentration, the sheet resistance or the mobility. In addition, Platz gives data on several coatings that were deposited on glass instead of on a-Si which affects the deposition conditions and therefore the quality of the TCO layer. Therefore, it is not straightforward to give an interpretation of their results.

	Emissivity (Affolter)	Emissivity (Platz et al)
ZnO on aSi	30%	41% (on glass?)
SnO2 on aSi	-	17% (on glass!)
ITO on aSi	42%	60%-65%
p-type Si	-	40%

Table 10: Emissivity of various PV types

In his paper, Platz proposes an optimized structure of the PVT cell as shown Figure 23.

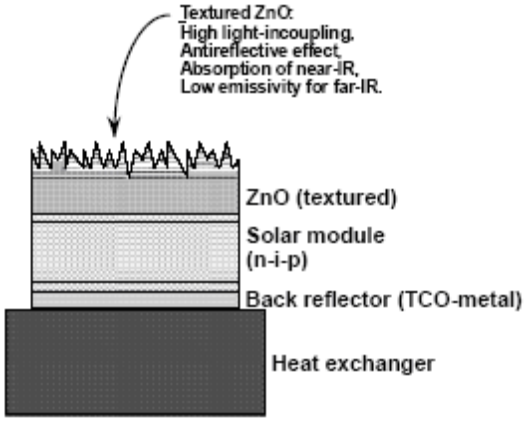

Figure 23: Thermally optimised a-Si PVT cell as presented by Platz (1997).

Two major practical complications for such a concept exist. This is due to the fact that the glass top surface has two important functions, that now have to be solved in another way

- For a-Si glass-glass modules, the top glass surface is the surface on which the layers are deposited, while the rear glass is laminated afterwards to the sandwich by means of e.g. EVA. Also a-Si flexible thin-film modules are available, in which the layers are deposited in reversed order on a flexible substrate, but it should be realized that it is not straightforward to reverse the order of deposition, which is mainly problematic due to the temperature of the various deposition steps and the effect this has on (diffusion in) already deposited layers. The reduced deposition temperature for the TCO leads to a reduced mobility, and therefore a lower TCO quality, including an increased emissivity. Also, differences in thermal expansion between the active material and the rear foil are problematic. For CIS, the back contact is deposited on the rear glass, after which the cells are deposited. This means that the TCO surface is deposited last and (normally, but not in our case) laminated to a top glazing.
- The glass protects the active PV from moisture. This is especially important for a-Si that degrades very fast under the effect of moisture, but also for c-Si moisture is problematic as it may lead to corrosion of contacts and possible degradation of the antireflection coating. It may be expected that this will seriously compromise the life time of the module. Therefore, in such concepts, especially when thin film cells are used, the space above the absorber needs to be sealed perfectly over the lifetime of the module.

5.2 Emissivity of PV material

In Table 10, the emissivity of p-type c-Si and various TCO's on a-Si was presented, as measured by Affolter and Platz.

- For the p-type c-Si, Platz reports a value of 40% emissivity. Unfortunately, Platz does not report the sheet resistance of the cell. Van Zolingen (2008) indicates that, since the mid 1990's, sheet resistance for p-type c-Si have been lowered substantially, resulting in lower emissivity. Van Zolingen (2008) gives 60% as a typical emissivity for modern cells, but indicates that for the future this will probably increase to even higher values, thereby reducing the difference between the emissivity of a encapculated and an unencapsulated cell. It can be concluded that under these circumstances the concept of an unencapsulated c-Si module is not very attractive.
- For the TCO coatings, Platz reports a low emissivity of 17% for SnO_2 on Asahi U-type glass and states that SnO_2 is already used as TCO for a-Si cells, which could make unencapsulated cell concepts interesting. However, Van Zolingen (2008) warns that the Asahi coatings are relatively thick and that this coating is deposited on glass instead of on a-Si, which allows for better deposition conditions than with deposition on a-Si, resulting in a higher mobility and a lower emissivity. For ZnO, Platz and Affolter find values in the range of 30-40%, and for ITO 40-65%. However, since the layer thickness, dopant level and mobility are not given, it is not easy to interpret these results. Van Zolingen (2008) indicates that 30-40% emissivity can be expected to be the lower limit that can be obtained in future disigns. Therefore, some reduction of the emissivity can be obtained in unencapsulated a-Si designs, but the reduction in emissivity is limited[b].

Finally, in order to make use of the low emissivity of the PV material, it is important that the surface is not covered by encapsulation material, since these generally have a very high emissivity.

a-Si Cells and Coatings	Absorptivity (a)	Emissivity (v)
Uncoated Solar Cell	0.70	0.56
Solar Cell w/ Urethane Hardcoat	0.67	0.81
Solar Cell w/ Hardcoat, .008 EVA, Tefzel	0.72	0.90
Solar Cell w/Hardcoat, Tefzel	0.73	0.87
Solar Cell w/Hardcoat, fiberglass	0.75	0.92

	Emissivity (Affolter)	Emissivity (Platz et al)
glass	88%-90%	86%
EVA (a-Si)	86%	-
Tefzel (a-Si)	95%	-

Table 11: (a) emissivity of USSC a-Si PV with various top encapsulants, (b) emissivity of a-Si cells with various top encapsulants.

5.3 Optical efficiency of unencapsulated PV

In order to evaluate the theoretical potential of using unencapsulated PV, simulation were carried out in matlab on the optical effect of leaving out the glass cover and the encapsulant. For the calculation, the data of a TiO_2 coating were used (no data were available of the nitride coating at that time, but the results are expected to be similar). The results are shown in Figure 24. The results indicate that in the optimum (corresponding to the peak in the AM 1.5 spectrum) the AR coating functions very well without glass, but at longer wavelengths the reflection seems to be somewhat higher. At the optimum, the reflection is reduced because the reflection at the air-glass interface has now disappeared, while the TiO2 also optically matches very well with the air-silicon interface. However, for longer wavelengths the TiO2 is optically matched better to the glass-silicon interface than to the air-silicon interface, resulting in higher reflection for the unencapsulated case.

[b] Possibly, due to the fact that CIS has a higher current density than a-Si (because it has a higher efficiency and lower bandgap), it will also have a higher dopant level, which will lead to lower emissivity than for a-Si. However, no confirmation for this could be found at the moment of the writing of this report.

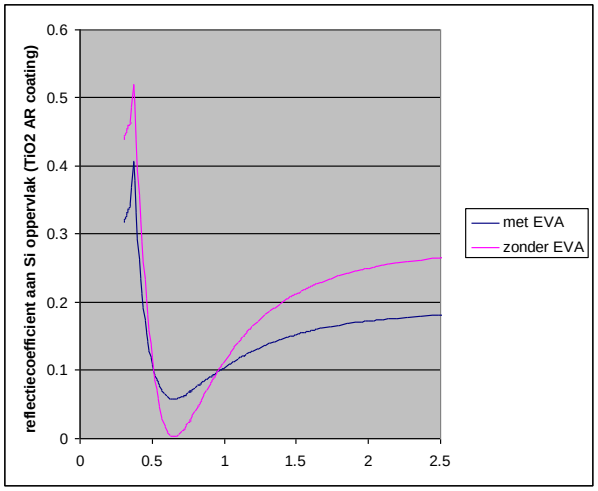

Figure 24: Calculated total reflection for Si-TiO2-EVA-air

A similar effect was also found in the literature for a nitride coating, as shown in Figure 25.

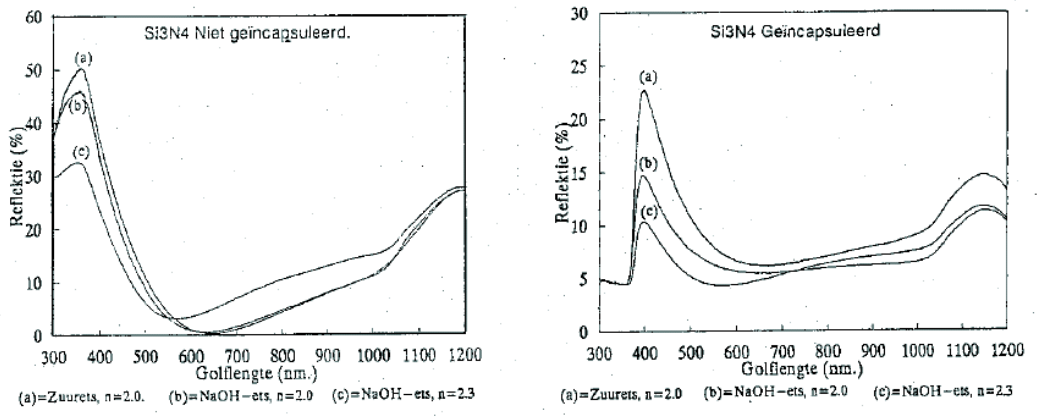

Figure 25: Effect of encapsulation on the reflection (from Michiels, Van Zolingen en Nijnatten, 1991).

5.4 Thermal module efficiency with unencapsulated cells

Next the thermal module efficiency was determined. In order to be able to calculate this, a number of assumptions was made:

- For the effective absorption factor, the information given in Table 12 by Van Zolingen (2006) was used. It was assumed that the application of different TCO's would not change the absorption as given in Table 12.
- For the emissivity of the various TCO's, the values were used that were presented by Platz and Affolter in Table 10. It was ignored that these emissivities may be too high since some of the measurements presented by Platz were actually for TCO deposited on glass. Therefore, the calculated values should be seen as an upper limit of the potential, since these values are probably not representative for TCO on thin film cells.
- Since no data were available for TCO on CIS, it was simply assumed that the emissivity of TCO on CIS would be equal to the emissivity of the same TCO on aSi.
- It was assumed that every TCO could be applied on every thin film cell, which may not be realistic.

Cell technology	Active area absorption factor (%)	Metallization concept	Total cell area absorption α_{th} (%)	PV cell efficiency η_{pv} (%)	$\alpha_{th} - \eta_{pv}$ (%)
Crystalline silicon					
- planar cells with Al back contact	80	H-pattern	75	13.5	61.5
- planar cells with diffusively reflecting back contact (Al)	85.6	H-pattern	80	14.0	66.0
- textured cell with diffusively reflecting back contact (Al)	90	H-pattern	85	15.0	70.0
			87	15.6	71.4
		PUM	90	16.2	73.8
- textured cell with diffusively reflecting highly absorbing back contact	93	EWT	90	15.0	75.0
			93	15.6	77.4
		PUM			
Amorphous silicon					
- structure with reasonable haze factor and reasonable optical confinement	72-75	EWT	70-73	5	65-68
- structure designed for optimal thermal absorption factor	84		82	7	75
CIS					
- structure with good haze factor and good optical confinement	91		89	12	77

Table 12: The active area, the total cell area and the effective absorption factor of various solar cell technologies (Van Zolingen et al, 2006).

The assumptions mentioned above resulted in the set of optical condition as presented in Table 13. These values were used to calculate the efficiency curves as presented in Figure 26. Because it was felt that both the electrical and the thermal output should be taken into account in one number, in order to be able to rank the different PV concepts, it was decided to plot the primary energy output (taken as thermal output + 2.5 times the electrical output) and divide that by the incoming solar energy.

	Total cell area absorption	PV cell efficiency	ε	τα
referentie	85%	15%	90%	0.782
c-Si H-pattern	85%	15%	40%	0.782
c-Si EWT	90%	16.20%	40%	0.828
a-Si - ITO	82%	7%	50%	0.7544
CIS - ITO	89%	12%	50%	0.8188
a-Si - SnO2	82%	7%	20%	0.7544
CIS - SnO2	89%	12%	20%	0.8188

Table 13: Calculated PV configurations

Figure 26 shows clearly that a substantial gain can be obtained relative to the reference situation with encapsulated PV; c-Si cells give the best results, followed by CIS with SnO_2. However, two warnings should be given to these optimistic results:

- as stated before, these results should be seen as an optimistic upper limit since the emissivity of the TCO may be overestimated.
- what is not taken into account here is the effect of the temperature increase on the annual PV efficiency; if the average collector temperature would rise 10C, the c-Si PV efficiency is lowered by about 5% relative. Especially for large systems, this effect can offset a substantial part of the additional gains, as shown by Santbergen (2008). He finds that for a 3 m2 PVT SDHW system,

a low emissivity coating may increase the thermal efficiency by 9.4% relative, while reducing the electrical efficiency with 5.5% relative (3.7% coating transmission, 1.8% temperature effect). For a 12 m2 PVT SDHW system, the thermal increase is 6.5%, while the electrical loss is 10.8% (3.7% coating transmission, 7.1% temperature effect). Since the absolute thermal efficiency is about 3 times the absolute electrical efficiency, for small areas there is still a clear gain in primary energy yield, while for extremely large SDHW systems with areas as large as 12 m2 the coating actually lowers the primary energy yield.

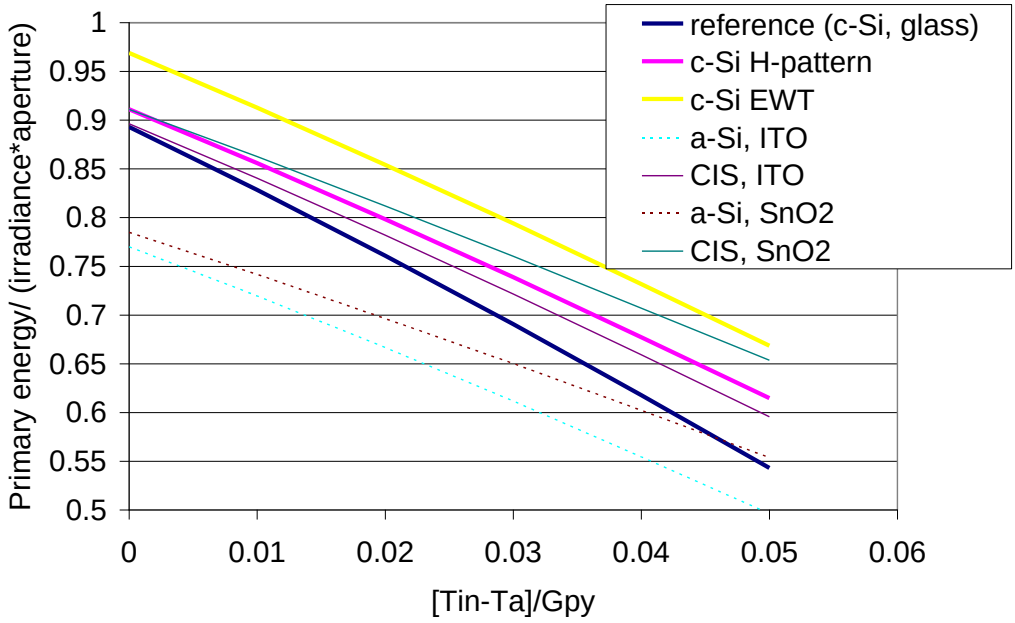

Figure 26: Primary energy efficiency for various unencapsulated PV cells.

In the present calculations only the effect of the low emissivity of the emitter on the crystalline silicon and the TCO on the thin film cells were investigated. An additional option for further lowering the heat loss by lowering the convective losses would be by application of noble gasses in the cavity instead of air. If one would use such a gas instead of air, this would further increase the thermal efficiency as indicated in Appendix B. However, this option was not investigated here.

5.5 Degradation of unencapsulated c-Si cells

Encapsulation of the cells is normally required to prevent degradation. For c-Si, in particular corrosion of the porous silvered contacts due to remaining acid solder flux combined with condensate could be detrimental (Kees Broek, pers comm.). Protection from corrosion is important especially as residual currents may be present. Also mechanical stress could be problematic since thermal expansion is not modified by the glass plate anymore, which may compromise the reliability of the contacts.
In order to have a first rough indication of the effect of cell degradation of unprotected cells, 4 unencapsulated PV cells were put in a standard collector casing during October 2007 - January 2008, and were flashtested at the start of the experiment, after two weeks in the outdoor collector casing (after which they remained indoors for some time before they were put back outside) and after another 4 weeks outdoors in the collector casing. The results are presented in Figure 27. Note that during the day, air temperatures of up to 50C were reached, while during night the temperature went down close to the freezing point and the relative humidity approached 90%. Unfortunately, cell no 7 broke while it was placed in the collector casing, so no measurements of this cell are available after 6 weeks. For the other cells, the results are not fully consistent; cell 4a shows a small efficiency increase (<1% relative), cell 5 a small efficiency decrease (<1.5% relative) and cell 4b a substantial decrease (<10% relative). During the second flash test, also in cell 4b a crack was found, which may be related to the degradation already apparent after the first measurement. Overall, some degradation was present, but this is relatively small and no clearly visible corrosion was present. However, for longer periods, it is still likely that substantially stronger degradation occurs for unencapsulated cells than for encapsulated cells.

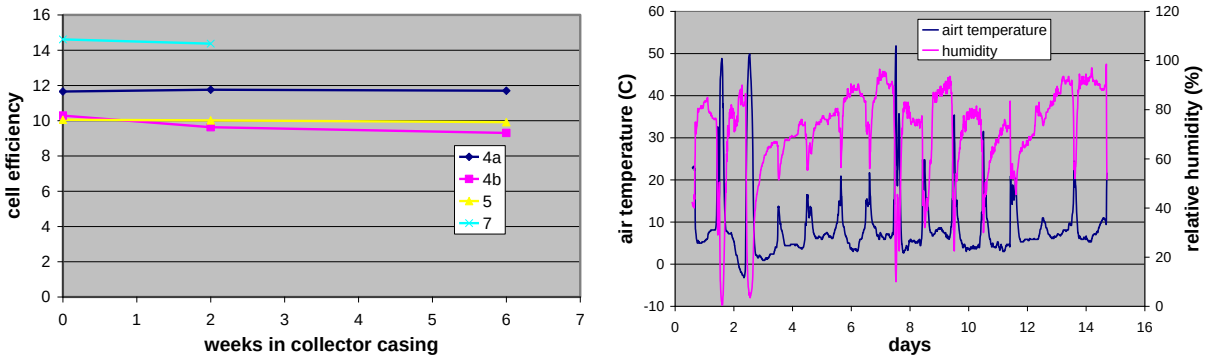

Figure 27: (a) Cell efficiency of unencapsulated cells after several weeks outdoors in standard glazed collector casing, (b) air temperature and humidity in collector casing (first two measurement weeks of period of figure (a)).

5.6 Experiences with a protective atmosphere

A means to prevent degradation of cells would be to put the in a protective atmosphere in which they are sealed from dust and moisture. Developments along these lines are taking place both in solar thermal collectors and in PV modules, as explained below.

5.6.1 Protective atmosphere in collectors

Very few examples exist of the application of a protective atmosphere inside a collector. Research on this topic already has a long history. Several publications were found from as early as 1980 about collector sealing and the effect of low pressure or noble gasses in the collector cavity or in between the double cover of a twofold covered collector (e.g. Malhotra, 1980; Zernial, 1980, Mendelsohn, 1980). More recent research was carried out at ZAE into Krypton-filled collectors (Benz and Beikircher, 1996) and on an evacuated flat plate collector for steam production (Benz and Beikircher, 1999), who indicated a slow loss of Krypton through the sealing.

Only two applications were found

- Buderus has commercialized a collector, in which the spacing above the collector is filled with Argon. This collector seems to be one of the main collector products of Buderus, and can therefore be expected to be extensively tested. Only very limited information on the construction of the collector could be found. For further information, see Appendix B.
- Thermosolar has developed a flat-plate vacuum collector. Since also ZAE was working on such a collector (Benz and Beikircher, 1999), possibly this is the same development. For further information, see Appendix B.

5.6.2 Protective atmosphere in PV modules

Unencapsulated PV is under development by various institutes. In these modules, the PV is encased between two glass plates that are sealed around the edge. An interesting example is the development of Lenhardt Maschinenbau, as described in Appendix D.

5.7 Recommendations for further testing

It is recommended to examine the possibilities of using cSi cells for unencapsulated PVT further. This includes measuring of actual emissivity values, optical measurements and reliability testing. It is expected that cSi cells have a relatively good resistance to moisture in the atmosphere compared to other PV techniques, but this should be examined further.
This leads to the following recommendations:

1. Optical measurements in which absorption and emission are measured over the entire relevant part of the spectrum.
2. Systems studies should be carried out to assess more thoroughly the potential benefits of the use of unencapsulated cells, also including the effect of temperature rise on PV efficiency.

If the above two investigations prove satisfactory, the reliability should be examined further:

3. Reliability testing is carried out in order to establish whether and under what conditions corrosion occurs or the nitride coating is degraded. This will also involve climate chamber testing with damp heat, combined with establishing changes in the IV characteristics. Thermal shock tests should be carried out in order to examine the mechanical stability.
4. The reliability of a protective atmosphere sealing should be examined. One option would be similar to the Buderus concept, while another could be similar to insulation glazing. Specific attention should be paid to high stagnation temperatures (compromising not only the reliability of the PV and the connections, but also leading to expansion of the gas in the enclosure). In addition, it may be interesting to use a drying agent such as silicagel to capture any moisture that has entered the enclosure (see also Mendelsohn, 1980), since condensation on the cells should be prevented also if the sealing may show some leakage.

6. Multicoating

6.1 Introduction

In the present PVT modules, crystalline silicium (cSi) cells are laminated to a commercial copper absorber by means of EVA. These absorbers have a (relatively costly) spectrally selective coating. Generally, such coatings have been optimized for the following aspects

- High absorption of solar radiation
- Low emissivity
- Thin layer (ensuring sufficient heat transfer)
- High temperature resistance up to stagnation temperature

However, in the present configuration, the spectral selectivity of the coating is not used, since the layers on top of the absorber are opaque to long wave irradiance. In addition, in order to make sure that no short-circuiting occurs between the copper absorber and the PV cells, the absorber is covered by an additional layer of Clear Tedlar, that is laminated to the absorber by means of EVA, which increases cost (Clear Tedlar is about 22 euro/m2, normal Tedlar 15 euro/m2, EVA 3,5 euro/m2, pers comm. Marcel Elswijk) and reduces heat transfer. In this paragraph, work is presented on the search for an alternative absorber layer, which has the following characteristics

- High absorption of solar radiation
- Electrically insulating
- Sufficient heat transfer
- High temperature resistance up to lamination temperature
- Low-cost

In order to determine their suitability as an absorber coating, measurements have been carried out on the following materials:

- Ceramics
- Polymers
- Paints

6.2 Literature study

6.2.1 Ceramics

In this paragraph, ceramics is defined as a compound of at least two elements, of which one is non-metallic. Examples are Al_2O_3 or SiO_2. These materials are often used because of their good electrically insulating characteristics and resistance to high temperatures. By using additives, the characteristics can be engineered further, which leads to a very large range of possible ceramic materials. The choice has been made to investigate here only the more common materials.
A disadvantage of ceramic materials is that these materials are brittle and have a low coefficient of thermal expansion compared to metals.

Material	Color	Melting point (°C)	Thermal conductivity (W/mK)	Electrical resistivity (Ω cm)	Special remarks*
Al_2O_3	White	2100	26-35	$>1x10^{14}$	-
MgO	White	2800	12.6	$>1x10^{12}$	-
TiO_2	White	1830-1850	2.5-5	$>1x10^{13}$	-
BeO	White	2570	260-300	$>1x10^{14}$	A5
CuO	Black	1204	?	$\sim 5x10^{-2}$	A3
Cu_2O	Red	1237	?	10^{9}-10^{12}	?
Cr_2O_3	Green	2300	?	?	?
ZrO_2	White	2710	2	$>1x10^{10}$	A3
SnO	Black	1080	?	?	?
Fe_2O_3	Red/ brown	1390	?	$38x10^{-3}$	-
FeO	Black	1369	?	?	?
AlN	Grey	2200	140-190	$>1x10^{14}$	A1-A3
BN	White	2500	71-121	$>1x10^{14}$	A3
Si_3N_4	Black	1900	30-35	$>1x10^{10}$	A3
SiC	Black/green	2300	120	10^{2}-10^{6}	A2-A3
B_4C	Black	2450	?	?	A2-A3
TiC	Light grey	3170	17.2	?	A2-A3
W_2C	Grey/black	2870	84	?	A3
Cu	Red	1083	401	$1.69x10^{-3}$	-

Table 14: Color, thermal conductivity and electrical resistively of common ceramic materials. For reference, also the values for copper are given. Special remarks: A1 – harmful, A2 – highly flammable, A3 – causes skin irritation, A4 – possibly carcinogenic, A5 – highly poisonous

The above table shows that resistance to high temperatures is not a problem for ceramics since melting temperatures are generally much higher than the required 150°C. Black colored ceramics are preferred since a darker coating absorbs more sunlight. However, it should be noted that non-black ceramics can be colored using additives and therefore the color is not a critical requirement.
A first selection was made by excluding all poisonous materials such as all nitrides and carbides, since the use of these materials will results in a increase in production process cost. Also electrically conductive materials were excluded, such as CuO and Fe_2O_3.
Based on the thermal characteristics of the materials, a final selection of three materials was made: Al_2O_3 was seen as the most interesting material, followed by TiO_2 and MgO. From interviews with manufacturers, however, it was found that Al_2O_3 couldn't be applied to copper substrates by conventional methods, while non-conventional methods would invoke substantial additional cost. Since aluminum absorbers are increasingly common (with copper tubing attached by laser-scribing), it was decided to investigate the application of an Al_2O_3 layer on an aluminum absorber.

6.2.2 Polymers

6.2.2.1 Introduction

A polymer is a large molecule that consists of at least two smaller units (monomers). These monomers can be identical or non-identical repetitive units. An example of identical repetitive units is PVC:

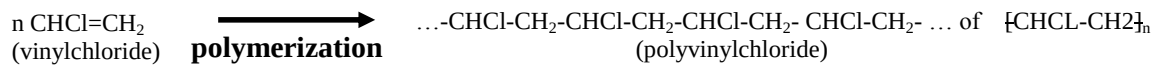

in which n is the degree of polymerization and has an integer value. A high temperature and/or UV radiation can trigger the polymerization. Two types of polymerization can be distinguished:

- Condensation polymerization, in which, apart from the polymer, also other products are formed (e.g. water).
- Addition polymerization, in which no additional products are formed.

In the present work, the focus will be on addition polymerization, because the formation of other products is problematic, as these will reduce the adhesion and the thermal conductivity.
At higher temperatures, the weak bonds in the polymer may be broken and subsequently join in a different way, thereby changing the characteristics of the polymer. This occurs for many polymers in the temperature range of 100-150 C. Exceptions are PTFE (also known as Teflon) and silicones, which will be examined further in the next paragraphs.

6.2.2.2 Xylan

Xylan is the main component of PTFE. It adheres very well to metals [17] and can be applied in layers of 5 micron. Fortunately, there was already substantial experience with Xylan[c] coating of metal surfaces within ECN, and test samples could easily be obtained. The Xylan coating on the test samples is dark green, but black Xylan is also commercially available.

6.2.2.3 Silicones

A large variety of silicones can be bought. Therefore, as a first step, manufacturers were asked to select silicones with a good thermal conductivity and a low electrical conductivity. This turned out to be difficult. Two manufacturers (Dow Corning and Lackwerke Peters GmbH) turned out to have suitable silicones that also had a good adhesion to metal. The application of the silicones proposed by Peters required various special facilities, so the choice was made to continue with the list supplied by Dow Corning as these were easier to apply.

Silicone type	Dyn. Viscosity (mPa.s)	Thermal conductivity (W/mK)	Electrical conductivity (Ω cm)
SE4400	76000	0,307	0,500
SE4451	32000	1,000	0,090
Q1-9226	50000	0,247	0,095
Q3-3600	4700	0,257	0,005
3-6605	47000	0,283	0,050
3-6751	10000	0,367	0,036
SE4410	3500	0,307	0,500
SE4447 CV	22000	0,833	0,410
SE4448 CV	102000	0,733	1,000
3-6651	32000	0,367	0,440
3-6652	34000	0,633	0,012
3-6655	33000	0,600	0,550

Table 15 Viscosity, thermal and electrical conductivity of Dow Corning 2-part silicones

The final selection of materials was then based upon the preference for 2-part silicones (additive reaction), and viscosities above 50 Pa*s[d] in order to have silicones that are sufficiently viscous to be easily applied. The largest realization potential was found for the 2-part silicones SE447 CV, 3-6655 and 3-6651 and these were chosen for further experimental research. In addition, also two 1-part silicones were selected for experimental research: Dow Corning (DC) 7091 and USEAL 500, which were selected based on their good resistance to high temperatures and their good adherence to metals.

6.2.3 Paints

Paints generally consist of three components: pigment, binder and solvent. In the hardening of the paint, the solvent evaporates and the binder cures or crosslinks. Several paints were chosen to be tested for the

[c] More specific: Xylan 1052
[d] 50 Pa s is about the viscosity of ketchup

applicability as an absorber in PVT panels. One of these paints was as special solar collector paint and 3 of these paints were regular epoxy based black paints obtainable in non specialized shops.

6.3 Experimental results

Based on the literature study, a number of materials were selected for further testing

1. One ceramic material: anodized aluminum (Al_2O_3)
2. Xylan
3. Silicones:
    a. Three 2-part silicones: SE447 CV, 3-6655 and 3-6651
    b. Three 1-part silicones: DC 7091 and USEAL 500
4. Paints

Of all these materials, a sample was made in which a coating of the selected material was applied to a substrate (15 cm × 15 cm). The substrate was a copper substrate of 0.3 mm in all cases except the anodized aluminum, for which an aluminum substrate with a thickness of 0.2 mm was used.
These materials were tested for

- Adherence to the substrate: visual inspection for Al_2O_3 and Xylan, adhesion test for silicones
- Resistance to a temperature of 150 C: visual inspection of heating in an oven for for 2 hours at 150 C.
- Electrical conductivity: In IEC 61215 a minimal electrical resistance of 40 MΩ is prescribed for a solar panel. In the present tests, 250 Volts DC was applied to the coating + substrate and the current was measured. The electrical resistance of the substrate itself was very low (less than 0.1 Ω) and could be ignored.
- Thermal conductivity: literature (Al_2O_3, Xylan 1052, paints) and by laser-flash testing of the diffusivity (silicones).
- The solar radiation absorptance was determined by measuring the reflectance between 0.4 to 1.75 μm and 1.9 to 2.5 μm using an integrating sphere.

In addition to the experimental results, the cost of the material is also reported. These costs were determined for the smallest tested layer thickness.

6.3.1 Ceramics

A 50-micron thick anodized black Al_2O_3 coating was applied to a 0.2 mm thick aluminum substrate. The 50-micron was the maximum thickness that was technically possible, which was chosen because of the brittleness of the anodization coating.

- **Adherence** Al_2O_3 forms a natural protective layer on aluminum to prevent further oxidation. The applied anodized black Al_2O_3 coating adheres therefore very good to the aluminum substrate.
- **Temperature resistance** With respect to the resistance to high temperatures, a sample was heated for 2 hours in an oven at 150 C. The temperature did not visibly affect the coating.
- **Electrical resistance:** It was found that the electrical resistance was larger than 300 MΩ (much larger than the 40 MΩ prescribed by IEC 61215).
- **Thermal conductivity:** From the literature, a value of 26-35 W/mK was found[e] for Al_2O_3.
- **Solar absorption:** An experimental solar absorptance of 0.78 was found for anodized black Al_2O_3.

[e] www.goodfellow.com/csp/active/static/E/Alumina.html

6.3.2 Xylan

In general, PTFE/Xylan have a small value for heat conductivity (for example, ~1000 times smaller than aluminum) and, consequently, PTFE/Xylan layers on non-stick frying pan are applied as very thin layers in order to conduct enough heat to fry the food. In addition to the low heat conductivity, very high costs are associated with applying thick layers of Xylan (0.5-1 mm). For these reasons, it was decided to apply thin layers with a thickness of 10, 25 and 50 micron on copper plates for testing purposes.

- **Adherence:** All three layers adhered very well to the copper substrate and could not easily be removed.
- **Temperature resistance:** A copper substrate with a 10-micron thick Xylan layer was heated in an oven for 2 hours at 150 C. No degradation was visible.
- **Electrical resistance:** It was found that the electrical resistance was larger than 300 MΩ (much larger than the 40 MΩ prescribed by IEC 61215).
- **Thermal conductivity:** From the literature, a value of 0.256 W/mK was found (Price, 2000) for PTFE (Xylan).
- **Solar absorption:** An experimental solar aborptance of 0.80 was found for dark green coloured PTFE/Xylan coating. Samples of PTFE/Xylan coated copper plates with thickness of 10 and 25 micron were used for the determination of the solar absorptance: both layer thicknesses gave the same value for solar absorptance.

6.3.3 Silicones

Several silicones were tested. Table 16 gives an overview of the silicones studied in this work:

Type	Kind	Color
SE4447 CV	2-part (1:1)	Grey
DC 3-6655	2-part(1:1)	Grey
DC 3-6751	2-part(1:1)	Grey
USEAL 500	1-part	White
DC 7091	1-part	Black

Table 16: Color of tested 2- and 1-part silicones

- **Adhesion** To test the adhesion of the silicones on copper, a layer of silicone with a thickness of a few millimeters was applied between two copper plates as shown in Figure 2:

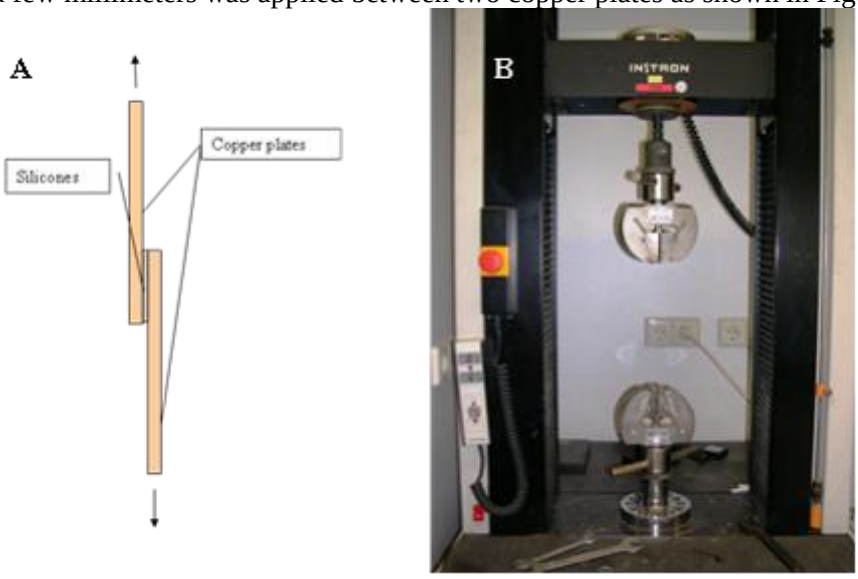

Figure 28: Testing adhesion of silicones on copper plate: A. sample configuration, B. Instron EH 489 Tensile testing equipment

The silicones were cured for one week at room temperature. The adhesion of the silicones on the copper was tested by pulling the two copper plates in opposite direction (see also Figure 28b) until the connection breaks: either at the copper-silicone interface or rupture of the silicone between the copper plates (without breaking the copper-silicone connection). Experimental force-displacement curves for the studied silicones are shown in Figure 29.

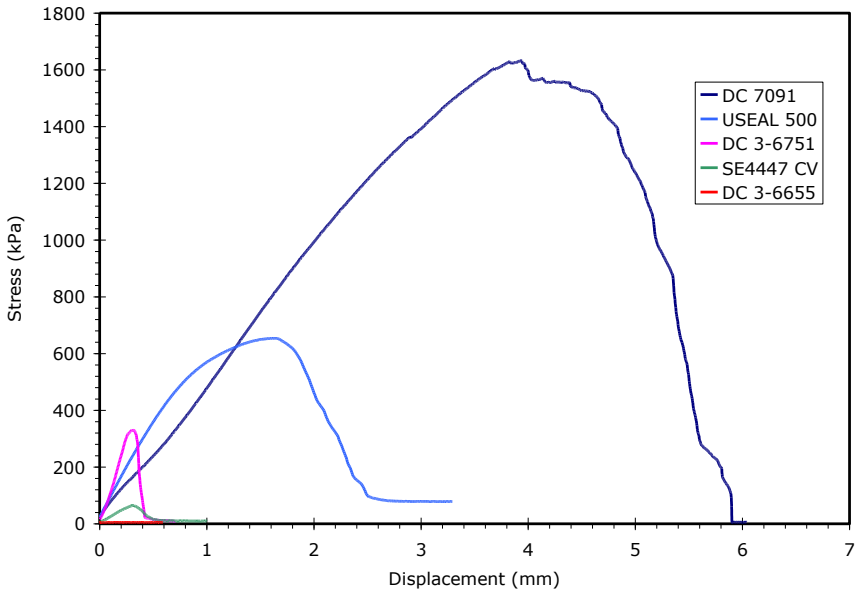

Figure 29: Results of adhesion test (see text for details)

In case of DC 3-6655 silicone, a viscous sticky fluid was formed after one week of curing, which did not adhere to the copper at all.

Figure 30: DC 3-6655 silicone after the adhesion test.

Consequently, the load-displacement curve (see Figure 29) shows a flat line. In all other cases, the load-displacement curve shows a gradual increase in load and displacement until a maximum load is reached. At the maximum load, the connection breaks: for DC 7091 and USEAL 500 the silicones rupture, while for DC 3-6751 and SE4447 CV the copper-silicone connection broke.

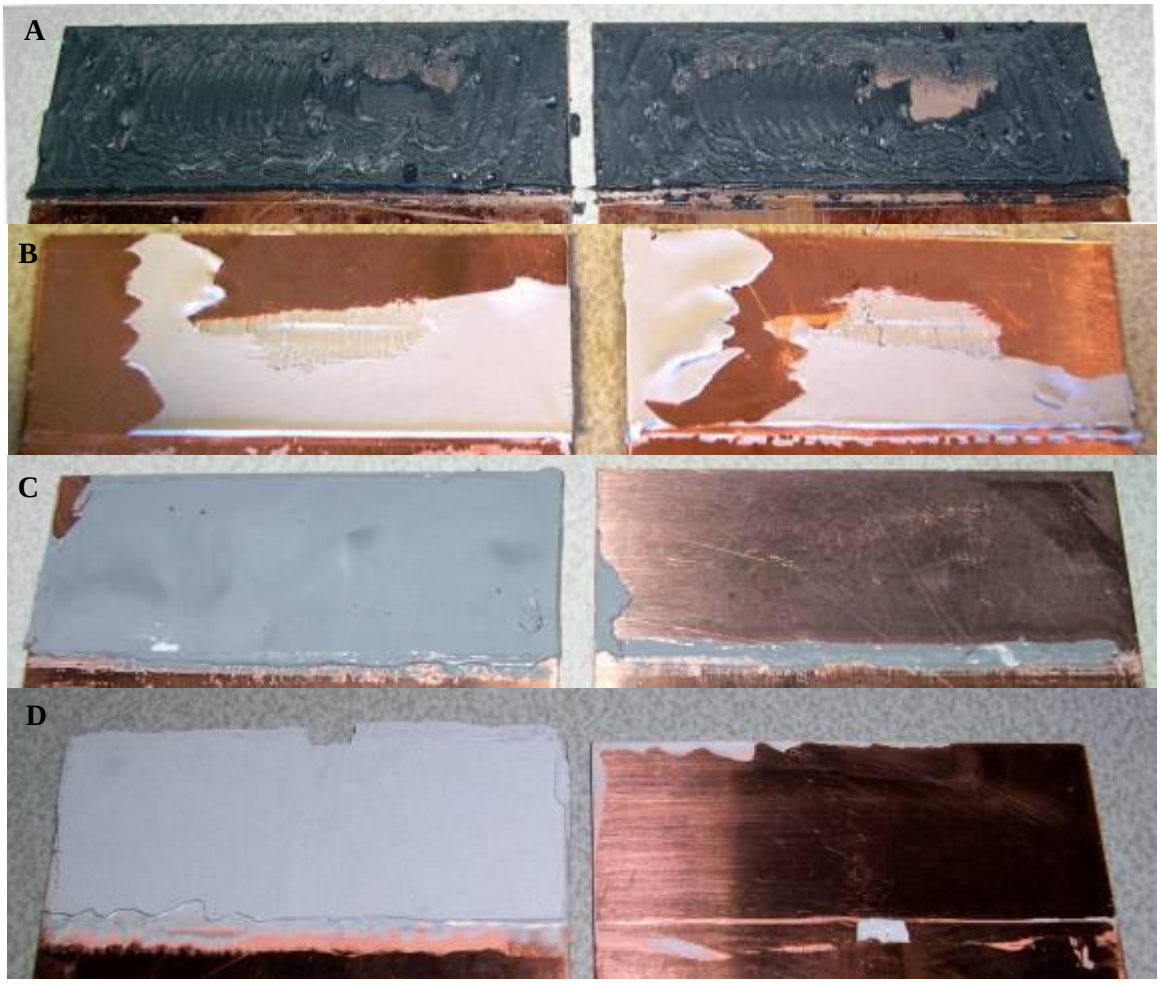

Figure 31: DC 7091 (A), USEAL 500 (B), SE4447 CV (C) and DC 3-6751 (D) silicones after the adhesion test.

It is surprising that the 2-part silicones (DC 3-6751 and SE4447 CV, see also Table 16) all show very low/weak adherence to the copper, while the 1-part silicones (DC 7091 and USEAL 500) show reasonable to good adherence. After curing for one week, a granular structure was found for some 2-part silicones that easily fell apart (see Figure 31), which explains the observed weaker adherence to copper.

In summary, the adhesion to copper depends strongly on the silicone: ranging from excellent (DC 7091) to (almost) no adhesion (DC 3-6655).

Temperature resistance: For all silicones, layers with a thickness of 60- or 240 micron were heated in an oven at 150 C for 2 hours. It was checked whether the layers showed discoloration, shrunk or burned. The temperature resistance of most silicones was generally very good. Only USEAL-500 was discolored and smelled as if burned.

A first selection can be made from the results of the above described adhesion and temperature resistance tests. The adhesion test clearly show that DC 7091 silicone adheres best to copper, while the temperature resistance test only indicated problems with USEAL-500 silicone. These results indicate that DC 7091 silicone is potentially a very good candidate for multicoating layer and therefore it was decided to save time and continue the remaining test only with DC 7091 silicone.

- **Electrical resistance:** The electrical resistance of the DC 7091 silicone was measured. It was found that the electrical resistance was larger than 300 MΩ (much larger than the 40 MΩ prescribed by IEC 61215).

- **Thermal conductivity:** Since the thermal conductivity of DC 7091 silicone is unknown, a set of experiments were performed to determine this quantity. The thermal conductivity is defined as $\kappa/\rho C_p$, where κ is thermal diffusivity (m^2/s), ρ is density (kg/m^3) and C_p = specific heat capacity (J/kg °C). Only the density is known (ρ=1397.2 kg/m^3), which means that both thermal diffusivity and specific heat capacity have to be determined experimentally. The diffusivity was measured using laser-flash method, while specific heat capacity was determined using differential scanning calorimetry. The results of these measurements are shown in Figure 32:

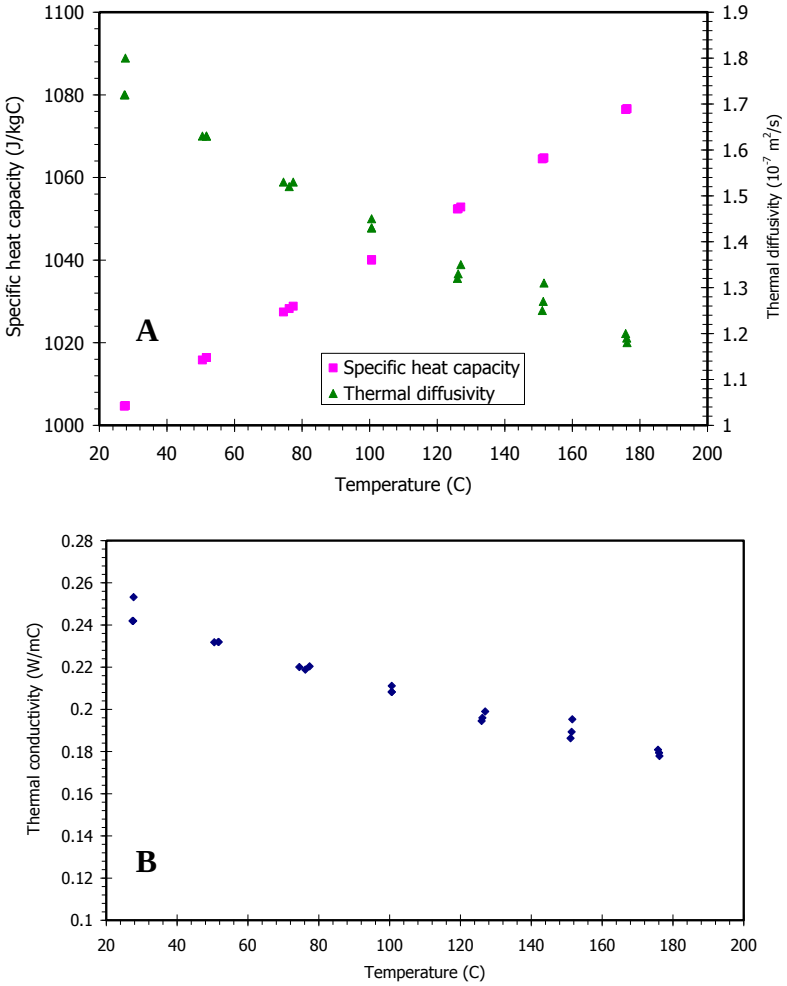

Figure 32A: Experimental thermal diffusivity and specific heat capacity of DC 7091 as function of temperature, B. experimental thermal conductivity of DC 7091 silicone as function of temperature.

The results show a small temperature dependence of the thermal conductivity in the temperature range of 20-200°C. The average value of the thermal conductivity (~0.20 W/m°C) is of the same order as the Xylan sample.

- **Solar absorption:** An experimental solar aborptance of 0.96 was found for DC 7091 coatings.. Samples of DC 7091 coated copper plates with thickness of 60 and 240 micron were used for the determination of the solar absorptance: both layer thicknesses gave the same value for solar absorptance.

6.3.4 Paints

Figure 33 shows the four paints which were tested in this study.

Figure 33: The four tested paints

One of these paints was as special solar collector paint and 3 of these paints were regular epoxy based black paints obtainable in non specialized shops. Table 17 gives an overview of the paints.

Type of paint	Solvent
Blackboard paint	VOC
CWS	VOC
Heat resistant paint	VOC
Solar collector paint	Water

Table 17: Tested paints
VOC = volatile organic compound

- **Solar absorption**: The values found for the absorptance are given in Table 18:

Type of paint	Absorptance
Blackboard paint	0.96
CWS	0.96
Heat resistant paint	0.95
Solar collector paint	0.95

Table 18: overview of absorptance for the four tested paints

All four tested paints show a high absorptance.

- **Temperature resistance**: tests were performed on the heat resistance of the paint by heating the paint to a temperature of 150 ^{o}C for about 2 hours. All paints performed well and showed no sign of degradation or change in properties (optically).

- **Electrical resistance**:
The measured electrical resistance are given in the table below.

Type of paint	Resistance
Blackboard paint	>300 MΩ
CWS	<0.1 MΩ
Heat resistant paint	< 0.1 MΩ
Solar collector paint	< 0.1 MΩ

Table 19: overview of measured resistance for the four tested paints

A specific resistance value between 0.1 MΩ and 300 MΩ was not obtained and the measurements resulted only in the extremes of conduction and insulation. Conduction in the blackboard paint was not obtained even after many attempts in which the electric contact point were pressed into the paint. Conduction for solar paint was measured at every attempt. For the other

paints, electrical conduction was not always measured and sometimes these paints show perfect isolation but these situations seemed to be a matter of luck. Electrical resistance is a key property of the collector paint and therefore only blackboard paint will be further investigated. The other paints are not applicable for PVT solar collectors.

- **Adhesion**: to test the adhesion of the blackboard paint to a copper plate, similar experiments were performed as were performed on the silicones. A layer of paint with was applied between two copper plates as show in Figure 28. The paint was for a week at ambient conditions. The adhesion of the paint to the copper was tested by pulling the two plates in the opposite direction. The force-displacement results of the adhesion test for the blackboard paint are given in the figure below.

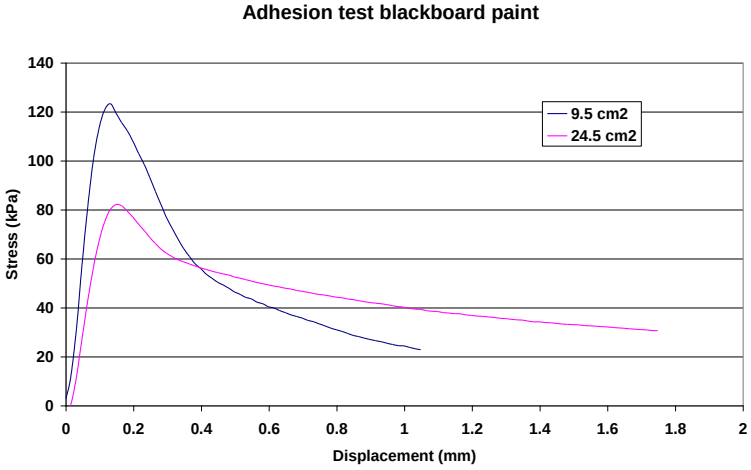

Figure 34: Force-displacement graph for blackboard paint.

The blue graph line was performed on a surface of 50x19mm and the pink graph line on a surface of 50x49mm.

- **Thermal conductivity**
  The thermal conductivity properties of the blackboard paint was deduced from the constituents of the epoxy paint. The results of epoxy paints show a thermal conductivity between 0.44 W/mK and 0.55 W/mK for dry and cured paints respectively.

6.4 Cost of materials

Table 20 shows the cost per collector area for the three tested materials, Clear Tedlar and EVA:

Material	Minimum tested layer thickness (μm)	Cost per collector area exlc. VAT (€/m^2)
Al_2O_3	50	137.5*
DC 7091	60	0.90
Xylan	10	0.38
Blackboard paint	60	1.00**
Clear Tedlar	100	22
EVA	500	3.5

*** = including price for deposition of layer on material**
**** = estimate on paint prices/area covered**

Table 20: Minimum tested layer thickness and costs (without VAT) for Al_2O_3, DC 7091, Xylan, Clear Tedlar and EVA.

It should be noted that the cost of Al_2O_3 includes the cost for depositing the Al_2O_3 layer on the aluminum substrate (including labor). Clearly, DC 7091 and Xylan are both considerable cheaper than EVA and Clear Tedlar.

6.5 Conclusions and recommendations for further research

The research presented in this chapter is focused on finding an alternative absorber layer, which has to have the following characteristics: cheap, high absorption of solar irradiation, electrically insulating, heat conducting, good adhesion and resistant to laminations temperatures of 150 °C.
Potential candidate materials for the alternative absorber layer are ceramics, polymers and/or paints. Based on a literature study and initial experiments three materials (Al_2O_3, DC 7091, Xylan and blackboard paint) were selected. These materials were further experimentally investigated.

Table 21 gives an overview of the experimental results and the cost of material for the three tested materials:

	adherence	Temperature resistance: 2 hours at 150°C	Electrical resistance (MΩ)	Thermal conductivity (W/mK)	Solar Absorptance	Cost excl. VAT (€/m^2)
Al_2O_3	Good	Passed	> 300	26-35	0.78	137.5*
DC 7091	Good	Passed	> 300	0.20	0.96	0.90
Xylan	Good	Passed	> 300	0.256	0.80	0.38
BB paint	Bad	Passed	> 300	0.44 – 0.55	0.96	1.00**

*** = including price for deposition of layer on material**
**** = estimate on paint prices/area covered**

Table 21: Overview of test results and cost of material for the Al_2O_3, DC 7091 and Xylan.

The results in the above Table show that all materials except blackboard paint show good adherence to the substrate. All materials are electrically insulating and are able to resist 150°C for 2 hours. Black anodized aluminum oxide (Al_2O_3) has the highest thermal conductivity of the three materials under investigation, but is also the most expensive material. DC 7091, Xylan and blackboard paint all had low material costs. These materials also showed similar low values for thermal conductivity (0.2-0.55), but since the layer thickness is very thin (10 – 60 micron), the effective heat transfer is of the order of 3000-10000 W/m2, which is far better than the minimum requirements. The solar absorption for the DC 7091 is considerably higher than for Xylan and based on these results, DC 7091 seems to be the best candidate for an alternative absorber layer.
However, it should be noted that the tested Xylan layer had a dark green colour. It is therefore recommended also to investigate the solar absorptance of a black coloured Xylan layer, which may result in a better solar absorptance. Similarly, adherence of blackboard paint directly to copper was bad but possibly a primer could be found to establish a better connection.
Finally, since the PVT modules are laminated to the (alternative) absorber by means of EVA, it is recommended to test the adherence of the three materials (Al_2O_3, DC 7091 and Xylan) to EVA.

7. Conclusions

This report describes an inventory of the various directions in which PVT modules could be improved and estimates the potential of these options. Investigated issues are

- Improved cell absorption
- Reduced glazing reflection
- Glass coatings to reduce radiative loss
- Unencapsulated cells for reduction of radiative loss
- Multicoatings for absorption, electrical insulation and optimised heat transfer
- Thin film options

It should be emphasized that this report focuses on the theoretical potential of these techniques, and only very limited experience is obtained on how these measures would affect the long-term reliability of a PVT collector. All of the above indicative studies would require further research on prototype level, and especially durability testing, before the technique should be considered for implementation.

The following conclusions can be drawn.

- Cell absorption of non-textured c-Si cells is already quite good (80-85%), but can be increased to 90% by texturing. Therefore, the use of textured cells is recommended. Furthermore, it is recommended to use cells with minimal metallic top grid area, since metallic top grid increases reflection losses. Therefore, the use of EWT cells is recommended, since the use of such cells would increase both the electrical and the thermal performance of a PVT module.
- For thin film options, CIS has the best absorption, which can be as high as 91%, provided that good confinement is obtained. For a-Si, also assuming good confinement, 84% absorption can be obtained, but for non-optimal confinement this is strongly reduced. The free carrier absorption has an important effect, and is responsible for 12% (CIS), 16% (c-Si) or even 19% (a-Si) of the light absorption in cells with good confinement.
- It was concluded that all CIS modules presently available are based on CIS deposited on the rear glazing (soda lime glass, which improves the CIS performance). Therefore, at present, the only option would be to glue a CIS module with the glass side to the metal absorber of the PVT. It is expected that this will lead to substantial problems related to the thermal expansion of the module, and that a relatively thick layer of flexible adhesive would be required between the metal and the glass to accommodate the stresses involved, thereby reducing the heat transfer. For the future, it would be interesting to follow the developments of flexible CIS modules that are now under development.
- The use of glazing with high transmission as produced e.g. by Flabeg is strongly recommended, since it increases both the electrical and the thermal efficiency. Also, some additional calculations were carried out for high transmission double glazings, to optimize the thermal performance. It was found that this indeed improves the thermal performance substantially, but the stagnation temperature becomes very high compromising the reliability of the PVT and also the average temperature rise will reduce the annual electrical efficiency, similar to the temperature effect of a low emissivity coating as indicated by Santbergen (2008).
- The use of low-emissivity SnO2 coatings on the glazings increases the thermal performance but reduces the electrical performance, which is due both to reduced transmission to the cells and increased average cell temperature (Santbergen, 2008). In terms of primary energy, a small nett positive effect of the coating can be obtained, provided that the thickness of the coating is optimized. However, it is doubtful if the small increase in yield justifies the added expense and more complicated manufacturing process. Other coatings are not expected to improve this situation; metallic coatings tend to have a much higher reflection and are therefore not considered suitable for PVT. ZnO and ITO coatings are not yet used on large glass surfaces, which is why

they were not examined in the present research. However, it is expected that these will not perform better than SnO2.

- Unencapsulated cells could in principle be used to reduce the radiative loss. The calculations for typical mid-90's PV cells indicate that in principle this technique could substantially increase the performance of a PVT collector. However, two big issues need attention;
    - Since the mid-90's sheet resistances have strongly increased and correspondingly cell emissivity has also increased, increasing the radiative loss of the base cell. Also for thin film there is reason to believe that the limited data found in the PVT literature (Platz, 1997; Affolter, 2000) are too optimistic because some of the data were measured on coated glass, which leads to a better layer quality than on a-Si. It seems that best realistic values for the emissivity are 60% for c-Si cells and 30-40% for a-Si cells. This severely limits the potential for this technique, but still a significant positive effect on the overall yield of the PVT could be obtained.
    - An important function of the encapsulation of the cells is to prevent these from moisture. Especially a-Si cells are highly sensitive to moisture and only if the collector casing around these cells can be sealed extremely reliably this could be seen as an alternative for conventional encapsulation. However, it is highly doubtful if this is a realistic option. For CIS, no data were obtained on the sensitivity to moisture, so it is not possible to draw conclusions for this technique, but the use of Cd in these cells may be an issue. For c-Si, the sensitivity to moisture of the cells is substantially less than for a-Si. Nevertheless, good sealing is important to protect the antireflective coating and prevent corrosion of contacts, especially if residual soldering flux is present.
- Multicoatings are an interesting option to improve the thermal contact between the PV and the solar thermal absorberplate, since they reduce the need for (expensive) additional layers of electrically insulating material and thereby reduce the overall thermal resistance as well as the overall cost. In addition, if such a coating would be available, this would be an alternative to the commercially manufactured spectrally selective solar thermal absorbers that are used now, potentially reducing the absorber cost. A number of coating materials was examined and the best material found was a one-component black silicone (DC 7091), with roughly the same cost as blackboard paint (about 1 euro/m2) and a much better adhesion. This coating is much cheaper than e.g. an additional layer of clear tedlar and EVA, which together cost about 25 euro/m2. The thermal resistance of a silicone coating is about 0.2 W/mK, which means that for the minimal coating thickness measured (60 microns), a heat transfer of almost 3500 W/m2 can be obtained, which is very good. In addition, the electrical resistance was measured to be larger than 300 MΩ (much larger than the 40 MΩ prescribed by IEC 61215). As alternative candidates to the silicone coating, it was indicated that blackboard paint could be interesting if the adhesion to copper could be improved with a suitable primer. In addition, a xylan coating could be interesting if the absorption could be improved with blackening additives. The overall conclusion is that multicoatings can be an interesting option for PVT, both to reduce cost and to increase heat transfer and that suitable materials have been identified.

8. References

1. Affolter, P., Haller, A., Ruoss, D., Toggweiler, P. (2000), New generation of hybrid solar PV/T collectors, report DIS 56360 / 16868
2. Affolter, P., Haller, A., Ruoss, D., Toggweiler, P. (2000), A new generation of hybrid solar collectors - Absorption and high temperature behaviour evaluation of amorphous modules, 16th EPSEC Glasgow.
3. Archer, M.D. and Hill, R. (2001), Clean Electricity from photovoltaics, Imperial college press.
4. Benz, N., Beikircher, T. (1999), High efficiency evacuated flat-plate solar collector for process steam production, Solar Energy 65(2), pp. 111-118.
5. Benz, Beikircher, Aghazadeh (1996), Aerogel and krypton insulated evacuated flat-plate collector for process heat production, Solar Energy 58(1-3), pp. 45-48.
6. Hadorn (2005), Thermal energy storage for solar and low energy buildings, IEA SHC task 32 publication.
7. Gordon (2001), Solar Energy The state of the art – ISES position papers, James & James.
8. Haitjema (1989), Spectrally selective tinoxide and indiumoxide coatings, PhD thesis TU Delft.
9. Malhotra, Garg, Rani (1980), Minimizing convective heat losses in flat plate solar collectors, Solar Energy, Vol 25, pp. 521-526.
10. Mendelsohn (1980), Collector sealants and breathing, report DOE.
11. Platz, R., Fischer, D., Zufferey, M.A., Anna Selvan, J.A., Haller, A., Shah, A. (1997), Hybrid collectors using thin-film technology, 26th PVSC Anaheim, CA
12. Price, D.M., Jarrat, M. (2000), Thermal conductivity of PTFE and PTFE compsites, Proceedings 28th conference of The North American Thermal Analysis Society, 579-584.
13. Santbergen (2008), Optical absorption factor of solar cells for PVT systems, PhD EUT.
14. Zernial (1980), Development of a selective thin film and of a hermetically sealed flat plate solar collector with gas filling, Final Report, Dec. 1980 Flachglass A.G. DELOG-DETAG, Gelsenkirchen (Germany, F.R.). Beschichtungslabor.
15. Zolingen, R.J.Ch. van, Santbergen, R., Rindt, C.C.M. (2006), PVT combi panels with various solar cell technologies, TUE-WET report 2006.24.
16. Zolingen, R.J.Ch. van, Santbergen, R. (2008), Application of coatings in PVT collectors, TUE-WET report 2008-01.
17. www.whitfordww.com/design/xylan-substrates.html
18. www.iecee.org/ctl/equipment/pdf/pv/EL_IEC61215_Ed2_final.pdf
19. www.research-equipment.com/viscosity%20chart.html

Appendix A Calculations for CIS PVT module concepts

Calculations for the module thermal and electrical efficiency have been carried out in matlab. A comparison has been made of cSi, aSi and CIS, both for single and double glazed modules with either normal low-iron glazing (transmission 92%) or antireflective low-iron glazing (transmission 95.5%). The values for the absorption and electrical efficiency of the various cell types were taken from Table 12 (module absorption: CIS 89%, cSi 86%, aSi 82%, module electrical efficiency: CIS: 12%, cSi 14%, aSi 7%), while a very good thermal conductivity of 500 W/m2K was assumed for all panel types. For all modules, 90% emissivity was assumed, due to the glazing on top of the PV. The results are shown in Figure 35.

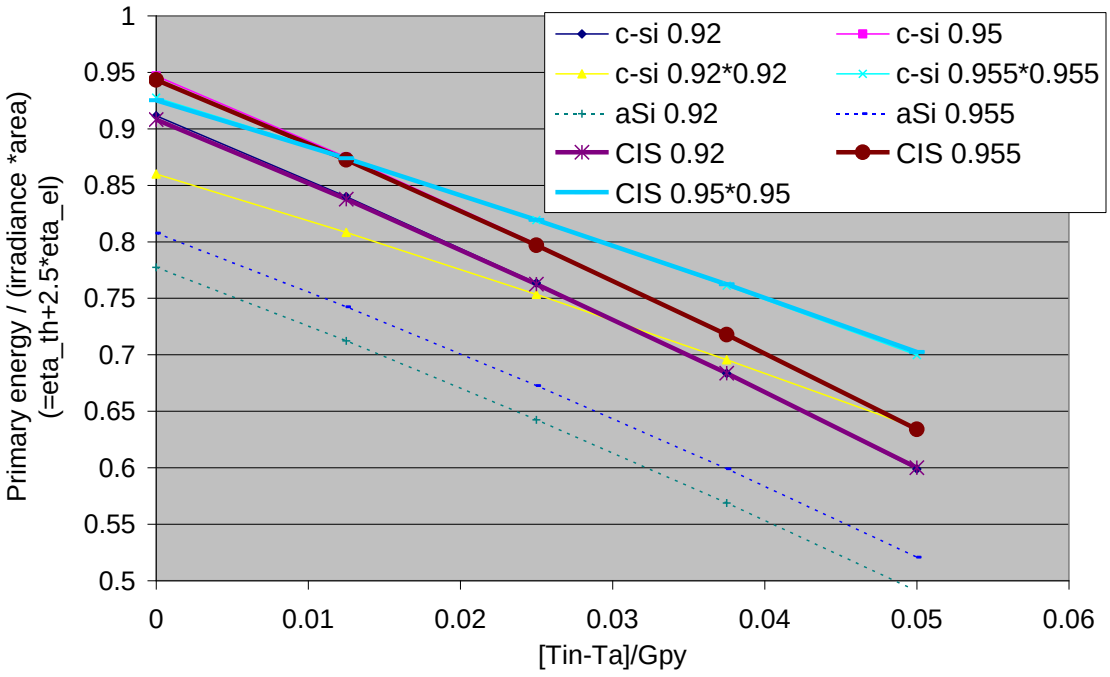

Figure 35: Primary energy yield per area for PVT modules with different PV types and glazing types.

It can be concluded that from the optical point of view, CIS is an interesting option, with an overall efficiency similar to cSi (provided that a good thermal contact can indeed be obtained, which is not trivial, given the considerations in the previous paragraph). The calculations further show that the option to use double layers of high transmission glazing would substantially improve the performance of the PVT modules, but only if there is a good method of reducing the stagnation temperature or an alternative encapsulant can be found, since the double glazing would also lead to high stagnation temperatures in the order of 160-170 °C, which is clearly too high for EVA. In addition, also here one should take into account the effect of the rise in average absorber temperature on the PV cell efficiency, which will reduce the electrical output. In Chapter 4, for a low emissivity coating, the rise in average absorber temperature is found to reduce the PV output significantly. To evaluate this effect for a double glazing, system performance calculations have to be carried out.

Appendix B Commercial CIS modules

The aim of this appendix is to give an overview of currently available CIS modules and their specifications. From the yearly module overview in Photon (issue February 2008) and an internet search, the following manufacturers of CIS modules were found:

1. Avancis (joint venture of Shell and Saint-Gobain Glass Deutschland)
2. Axitec
3. Global Solar
4. Schüco
5. Showa Shell Solar K.K.
6. Sulfurcell
7. Würth Solar

The products of these companies will be described below.

B.1 Avancis

From 1980 onwards ARCO solar had been investing in CIS module development. In 1990, Siemens took over ARCO solar, which was then the world's largest PV company, and in 1991 started a new CIS research program. In 1998, commercial production of CIS was started in the factory in Camarillo (California). Siemens Solar was taken over by Shell Solar in 2002 and continued to CIS development, as well as the sale of the CIS modules. In 2006 Shell sold all its c-Si activities to SolarWorld and decided to concentrate on CIS. Shell and Saint-Gobain Glass Deutschland have announced their joint venture, Avancis, whose 20 MW plant started production in 2008. (http://www.avancis.de)

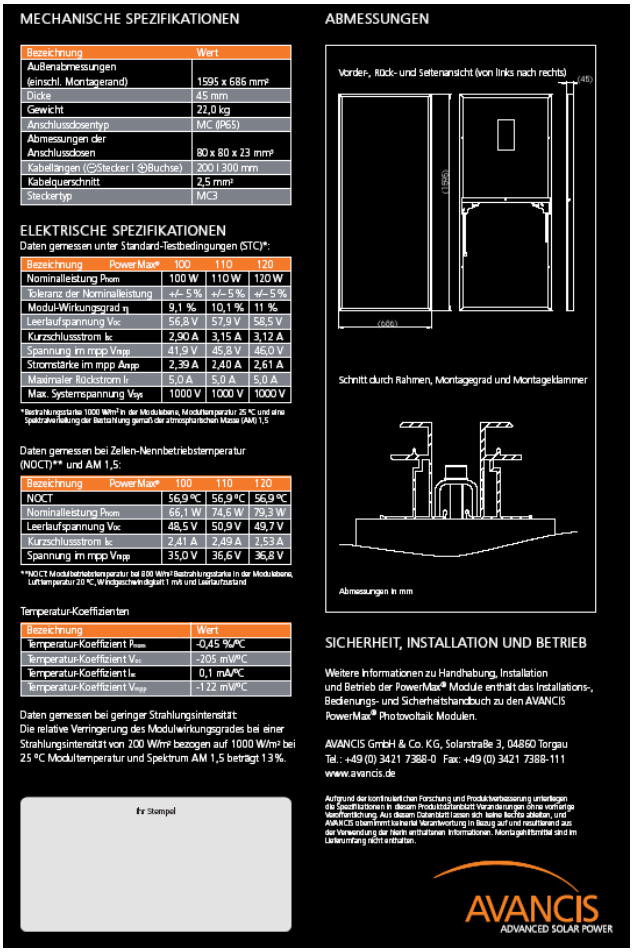

MECHANISCHE SPEZIFIKATIONEN

Bezeichnung	Wert
Außenabmessungen (einschl. Montagerand)	1595 x 686 mm²
Dicke	45 mm
Gewicht	22,0 kg
Anschlussdosentyp	MC (IP65)
Abmessungen der Anschlussdosen	80 x 80 x 23 mm²
Kabellängen (⊖Stecker I ⊕Buchse)	200 I 300 mm
Kabelquerschnitt	2,5 mm²
Steckertyp	MC3

ELEKTRISCHE SPEZIFIKATIONEN

Daten gemessen unter Standard-Testbedingungen (STC)*:

Bezeichnung PowerMax®	100	110	120
Nominalleistung P_{nom}	100 W	110 W	120 W
Toleranz der Nominalleistung	+/– 5 %	+/– 5 %	+/– 5 %
Modul-Wirkungsgrad η	9,1 %	10,1 %	11 %
Leerlaufspannung V_{oc}	56,8 V	57,9 V	58,5 V
Kurzschlussstrom I_{sc}	2,90 A	3,15 A	3,12 A
Spannung im mpp V_{mpp}	41,9 V	45,8 V	46,0 V
Stromstärke im mpp A_{mpp}	2,39 A	2,40 A	2,61 A
Maximaler Rückstrom I_r	5,0 A	5,0 A	5,0 A
Max. Systemspannung V_{sys}	1000 V	1000 V	1000 V

*Bestrahlungsstärke 1000 W/m² in der Modulebene, Modultemperatur 25 °C und eine Spektralverteilung der Bestrahlung gemäß der atmosphärischen Masse (AM) 1,5

Daten gemessen bei Zellen-Nennbetriebstemperatur (NOCT)** und AM 1,5:

Bezeichnung PowerMax®	100	110	120
NOCT	56,9 °C	56,9 °C	56,9 °C
Nominalleistung P_{nom}	66,1 W	74,6 W	79,3 W
Leerlaufspannung V_{oc}	48,5 V	50,9 V	49,7 V
Kurzschlussstrom I_{sc}	2,41 A	2,49 A	2,53 A
Spannung im mpp V_{mpp}	35,0 V	36,6 V	36,8 V

**NOCT: Modulbetriebstemperatur bei 800 W/m² Bestrahlungsstärke in der Modulebene, Lufttemperatur 20 °C, Windgeschwindigkeit 1 m/s und Leerlaufzustand

Temperatur-Koeffizienten

Bezeichnung	Wert
Temperatur-Koeffizient P_{nom}	-0,45 %/°C
Temperatur-Koeffizient V_{oc}	-205 mV/°C
Temperatur-Koeffizient I_{sc}	0,1 mA/°C
Temperatur-Koeffizient V_{mpp}	-1,22 mV/°C

Daten gemessen bei geringer Strahlungsintensität:
Die relative Verringerung des Modulwirkungsgrades bei einer Strahlungsintensität von 200 W/m² bezogen auf 1000 W/m² bei 25 °C Modultemperatur und Spektrum AM 1,5 beträgt 13 %.

Ihr Stempel

ABMESSUNGEN

Vorder-, Rück- und Seitenansicht (von links nach rechts)

Schnitt durch Rahmen, Montagegrad und Montageklammer

Abmessungen in mm

SICHERHEIT, INSTALLATION UND BETRIEB

Weitere Informationen zu Handhabung, Installation und Betrieb der PowerMax® Module enthält das Installations-, Bedienungs- und Sicherheitshandbuch zu den AVANCIS PowerMax® Photovoltaik Modulen.

AVANCIS GmbH & Co. KG, Solarstraße 3, 04860 Torgau
Tel.: +49 (0) 3421 7388-0 Fax: +49 (0) 3421 7388-111
www.avancis.de

AVANCIS
ADVANCED SOLAR POWER

Figure 36: Powermax CIGS module by Avancis

B.2 Axitec

From the website of Axitec, the recent leaflets are all cSi modules. The leaflets on CIS modules that can still be downloaded are under ‘altere Datenblättern’; it seems from this that Axitec has stopped its commercial CIS activities.

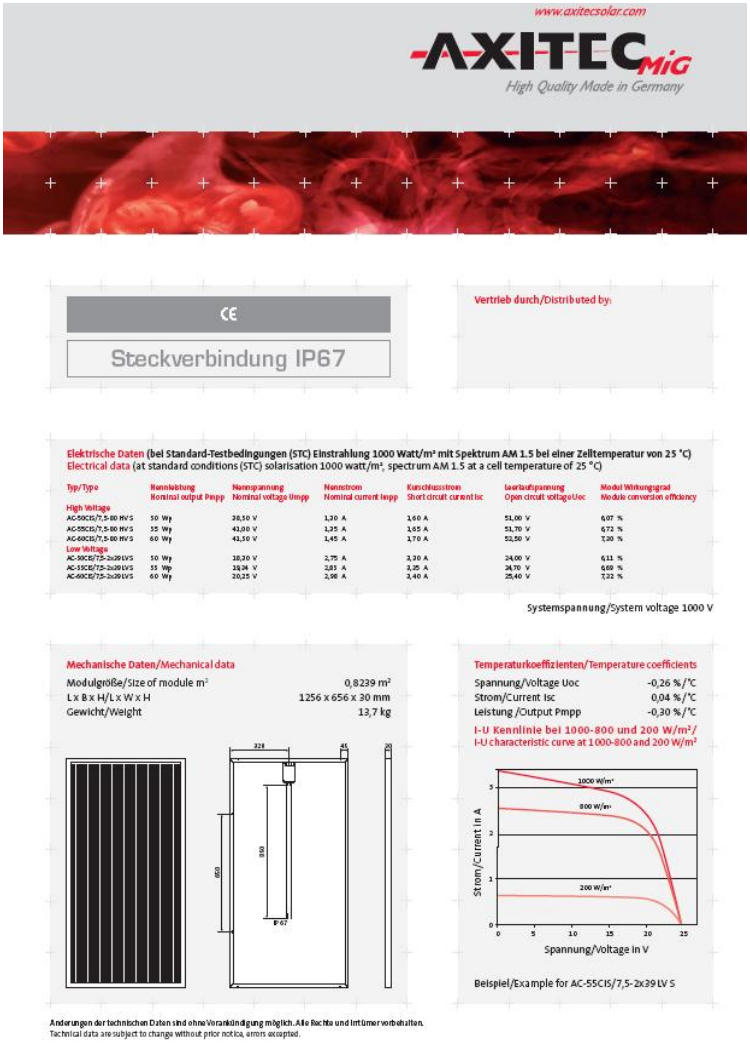

Figure 37: Axitec CIS modules\

B.3 Global Solar (USA)

Global Solar, Inc (http://www.globalsolar.com) is manufacturing CIS modules since 1996 and describes itself as the leading manufacturer on flexible CIGS modules. However, on their website only specifications of glass modules could be found.

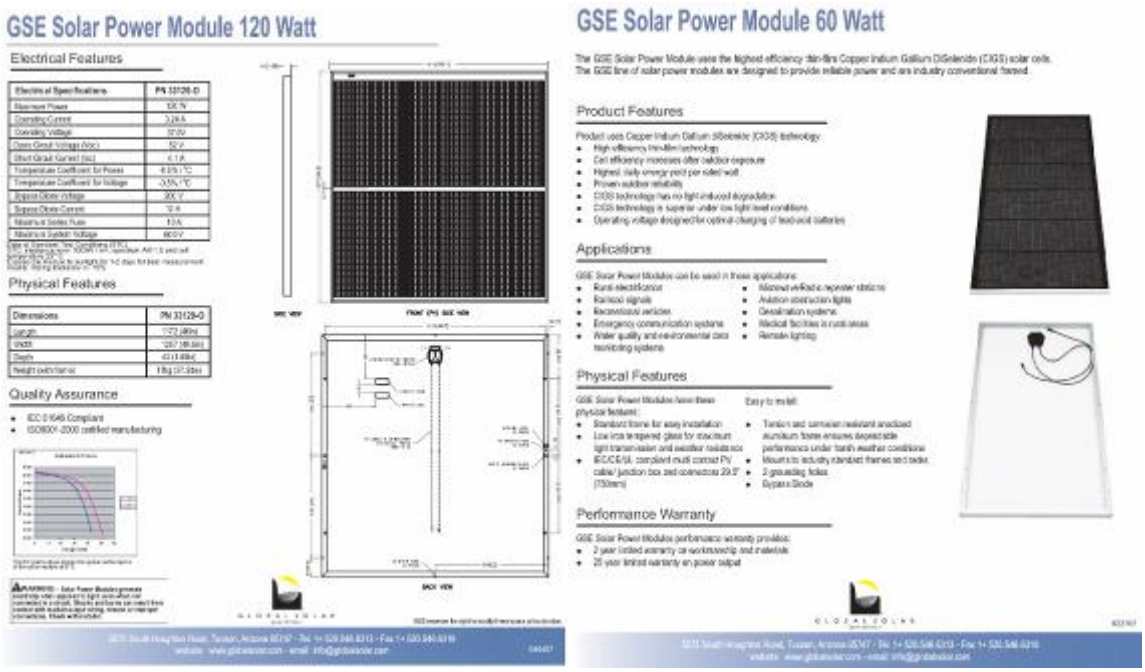

Figure 38: glass-glass CIS modules by Global Solar

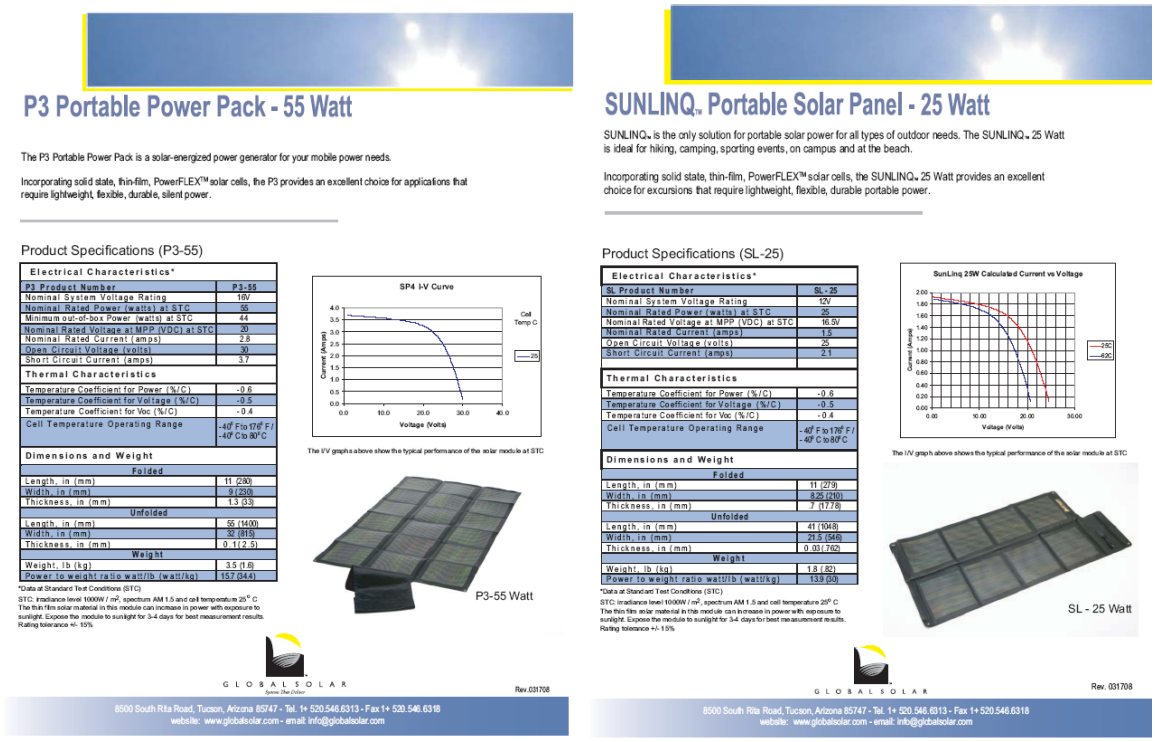

Figure 39: Flexible CIGS modules by Global Solar

B.4 Showa Shell Solar

The following information was found from www.showa-shell.co.jp:

Showa Shell Solar K.K., a 100% subsidiary of Showa Shell Sekiyu K.K., has decided to construct the second CIS photovoltaic module factory. The CIS photovoltaic module goes under the product name "SOLACIS". Showa Shell Solar K.K. has started commercial production after test production at its first Miyazaki Plant (construction completed in October 2006). This time, Showa Shell Solar K.K. has decided to construct the second factory with production capacity of 60 MW. The second factory will be

the world's largest CIS photovoltaic module factory. Products manufactured at this factory are planned to be sold mainly in domestic market, through Showa Shell Sekiyu K.K.'s agent network.

Although the site indicated that commercial production of CIS modules in the Miyazaki Plant started in 2007, no module specifications could be found. Also the Photon overview on CD-ROM did include Shell Showa as manufacturer, but did not present any module information.

B.5 Schüco

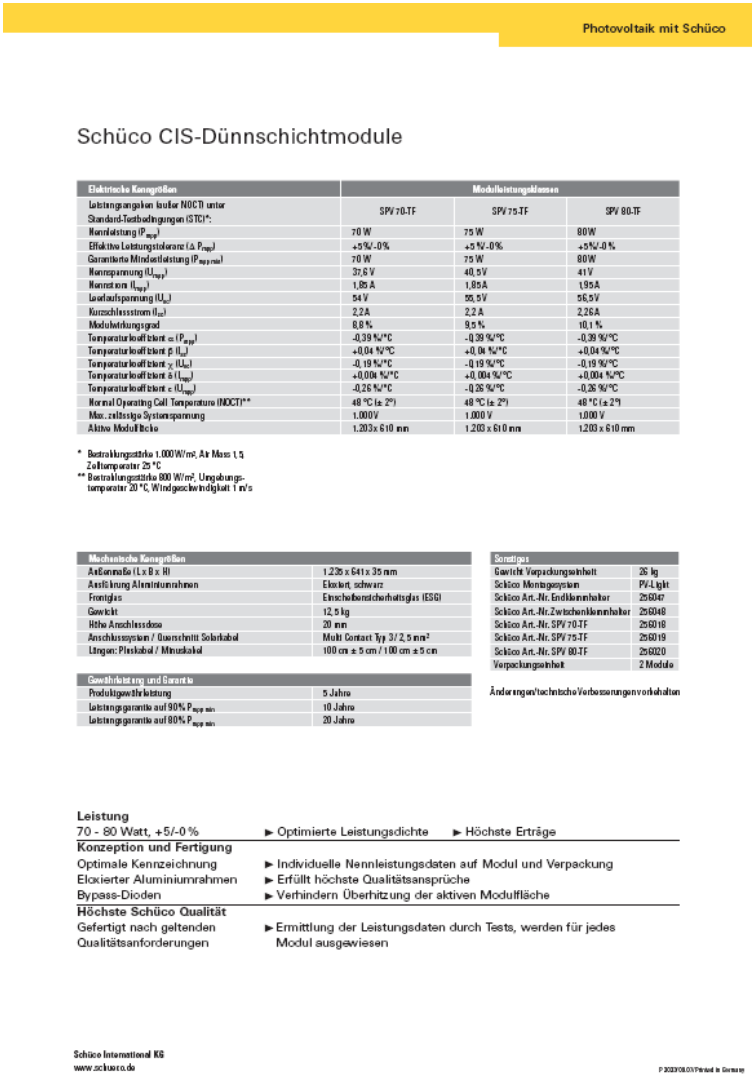

Photovoltaik mit Schüco

Schüco CIS-Dünnschichtmodule

Elektrische Kenngrößen	Modulleistungsklassen		
Leistungsangaben (außer NOCT) unter Standard-Testbedingungen (STC)*:	SPV 70-TF	SPV 75-TF	SPV 80-TF
Nennleistung (P_{mpp})	70 W	75 W	80 W
Effektive Leistungstoleranz (ΔP_{mpp})	+5 %/-0 %	+5 %/-0 %	+5 %/-0 %
Garantierte Mindestleistung ($P_{mpp\,min}$)	70 W	75 W	80 W
Nennspannung (U_{mpp})	37,6 V	40,5 V	41 V
Nennstrom (I_{mpp})	1,85 A	1,85 A	1,95 A
Leerlaufspannung (U_{oc})	54 V	55,5 V	56,5 V
Kurzschlussstrom (I_{sc})	2,2 A	2,2 A	2,26 A
Modulwirkungsgrad	8,8 %	9,5 %	10,1 %
Temperaturkoeffizient α (P_{mpp})	-0,39 %/°C	-0,39 %/°C	-0,39 %/°C
Temperaturkoeffizient β (U_{oc})	+0,04 %/°C	+0,04 %/°C	+0,04 %/°C
Temperaturkoeffizient γ (I_{sc})	-0,19 %/°C	-0,19 %/°C	-0,19 %/°C
Temperaturkoeffizient δ (I_{mpp})	+0,004 %/°C	+0,004 %/°C	+0,004 %/°C
Temperaturkoeffizient ε (U_{mpp})	-0,26 %/°C	-0,26 %/°C	-0,26 %/°C
Normal Operating Cell Temperature (NOCT)**	48 °C (± 2°)	48 °C (± 2°)	48 °C (± 2°)
Max. zeitstige Systemspannung	1.000 V	1.000 V	1.000 V
Aktive Modulfläche	1.203 x 610 mm	1.203 x 610 mm	1.203 x 610 mm

* Bestrahlungsstärke 1.000 W/m², Air Mass 1,5, Zelltemperatur 25 °C
** Bestrahlungsstärke 800 W/m², Umgebungstemperatur 20 °C, Windgeschwindigkeit 1 m/s

Mechanische Kenngrößen	
Außenmaße (L x B x H)	1.226 x 641 x 35 mm
Ausführung Aluminiumrahmen	Eloxiert, schwarz
Frontglas	Einscheibensicherheitsglas (ESG)
Gewicht	12,5 kg
Höhe Anschlussdose	20 mm
Anschlusssystem / Querschnitt Solarkabel	Multi Contact Typ 3 / 2,5 mm²
Längen: Pluskabel / Minuskabel	100 cm ± 5 cm / 100 cm ± 5 cm

Gewährleistung und Garantie	
Produktgewährleistung	5 Jahre
Leistungsgarantie auf 90% $P_{mpp\,min}$	10 Jahre
Leistungsgarantie auf 80% $P_{mpp\,min}$	20 Jahre

Sonstiges	
Gewicht Verpackungseinheit	25 kg
Schüco Montagesystem	PV-Light
Schüco Art.-Nr. Endklemmhalter	256047
Schüco Art.-Nr. Zwischenklemmhalter	256048
Schüco Art.-Nr. SPV 70-TF	256018
Schüco Art.-Nr. SPV 75-TF	256019
Schüco Art.-Nr. SPV 80-TF	256020
Verpackungseinheit	2 Module

Änderungen technische Verbesserungen vorbehalten

Leistung
70 - 80 Watt, +5/-0 % ► Optimierte Leistungsdichte ► Höchste Erträge

Konzeption und Fertigung
Optimale Kennzeichnung ► Individuelle Nennleistungsdaten auf Modul und Verpackung
Eloxierter Aluminiumrahmen ► Erfüllt höchste Qualitätsansprüche
Bypass-Dioden ► Verhindern Überhitzung der aktiven Modulfläche

Höchste Schüco Qualität
Gefertigt nach geltenden Qualitätsanforderungen ► Ermittlung der Leistungsdaten durch Tests, werden für jedes Modul ausgewiesen

Schüco International KG
www.schueco.de

Figure 40: Schüco CIGS module

B.6 Sulfurcell

A special type of CIS modules, not based on selenide but on sulfide (Cu-In-S instead of Cu-In-Se), is produced by Sulfurcell. Note that since the bandgap of these cells is much larger than the Se based CIS cells, these modules will probably have a much lower absorption than other CIS modules and will therefore be less suitable for PVT. Sulfurcell provides the following spec sheets:

	SCG50-HV	SCG55-HV	SCG60-HV
Nennleistung**	50 W	55 W	60 W
Toleranz	± 5 %	± 5 %	± 5 %
Modulwirkungsgrad	6,2 %	6,8 %	7,4 %
Spannung MPP*	37,5 V	39,2 V	41 V
Strom MPP*	1,35 A	1,4 A	1,48 A
Leerlaufspannung*	50,0 V	51 V	52,5 V
Kurzschlussstrom*	1,65 A	1,7 A	1,7 A
Leerlaufspannung bei -10°C*	54,5 V	55,5 V	57,2 V
Spannung im MMP bei 70°C*	33,5 V	35,0 V	36,7 V
Temperaturkoeffizient I_{sc}	-0,04%/K	-0,04%/K	-0,04%/K
Temperaturkoeffizient U_{oc}	-0,26%/K	-0,26%/K	-0,26%/K
Temperaturkoeffizient P_{max}	-0,30%/K	-0,30%/K	-0,30%/K
max. Systemspannung	1000 V	1000 V	1000 V
Höhe in mm	1256	1256	1256
Breite in mm	656	656	656
Dicke in mm	30	30	30
Rahmentyp	Aluminium	Aluminium	Aluminium
Gewicht	13,7 kg	13,7 kg	13,7 kg
Produktgarantie	2 Jahre	2 Jahre	2 Jahre

* Toleranz der elektrischen Parameter ± 10 %

** Ermittelt unter Standardtestbed.: 25 °C, 1000W/m², AM1.5

Datenblatt Typ SCG-LV

Modul	SCG50-LV	SCG55-LV	SCG60-LV
Nennleistung**	50 W	55 W	60 W
Toleranz	+ /- 5 %	+ /- 5 %	+ /- 5 %
Modulwirkungsgrad	6,2 %	6,8 %	7,4 %
Spannung MPP*	18 V	20 V	folgen
Strom MPP*	2,75 A	2,85 A	folgen
Leerlaufspannung*	24 V	25,5 V	folgen
Kurzschlussstrom*	3,3 A	3,4 A	folgen
Leerlaufspannung bei -10°C*	28,5 V	30 V	folgen
Spannung im MPP bei 70°C*	16 V	18 V	folgen
Temperaturkoeffizient $T_K(I_{sc})$	0,04 %/K	0,04 %/K	0,04 %/K
Temperaturkoeffizient $T_K(U_{oc})$	- 0,26 %/K	- 0,26 %/K	- 0,26 %/K
Temperaturkoeffizient $T_K(P_{max})$	- 0,30 %/K	- 0,30 %/K	- 0,30 %/K
max. Systemspannung	1000 V	1000 V	1000 V
Höhe in mm	1256	1256	1256
Breite in mm	656	656	656
Dicke in mm	30	30	30
Rahmentyp	Aluminium	Aluminium	Aluminium
Gewicht	13,7 kg	13,7 kg	13,7 kg
Produktgarantie	2 Jahre	2 Jahre	2 Jahre

* Toleranz der elektrischen Parameter ± 10 %

** Ermittelt unter Standardtestbedingungen: 25°C, 1000W/m², AM1.5

B.7 Würth CIS modules

Technische Daten

Über weitere Leistungsklassen informieren wir Sie gerne auf Anfrage

	WSK0001	WSK0039	WSK0019	WSK0020	WSK0021	WSG0036 E075	WSG0025 E080	WSG0035 E075
Nennleistung (P_{max}) in Wp	5,5	12,0	23,0	35,0	55,0	75,0	80,0	75,0
Systemspannung (V) in V	12,0	12,0	12,0	12,0	12,0	24,0	120,0	12,0
Spannung MPP (V_{mpp}) in V	16,5	16,5	16,5	16,5	16,5	35,0	120,0	16,5
Strom im MPP (I_{mpp}) in A	0,33	0,73	1,40	2,12	3,33	2,15	0,67	4,42
Leerlaufspannung (V_{oc}) in V	22,0	22,0	22,0	22,0	22,0	44,5	160,0	22,0
Kurzschlussstrom (I_{sc}) in A	0,35	0,78	1,50	2,29	3,56	2,36	0,72	5,01
Leerlaufspannung (V_{oc}) bei -10 °C in V	24,3	24,3	24,3	24,3	24,3	49,0	177,0	23,5
MPP-Spannung (V_{mpp}) bei +70 °C in V	13,8	13,8	13,8	13,8	13,8	29,3	101,0	14,2
Spannungsänderung pro °C (%)	-0,29	-0,29	-0,29	-0,29	-0,29	-0,29	-0,29	-0,29
Leistungsänderung pro °C (%)	-0,36	-0,36	-0,36	-0,36	-0,36	-0,36	-0,36	-0,36
Abmessungen in mm (H x B x T)²	205 x 305 x 31	405 x 305 x 31	405 x 605 x 31	605 x 605 x 31	605 x 905 x 35	605 x 1.205 x 35	605 x 1.205 x 35	605 x 1.205 x 35
Gewicht (kg)	1,3	2,4	4,5	6,5	9,7	12,7	12,7	12,7
Anschlussvariante (s. u.)	①	①	①	①	③	②	②	③

Die elektrischen Daten gelten für Standard Testbedingungen (STC): 1.000 W/m², AM 1,5, 25 °C

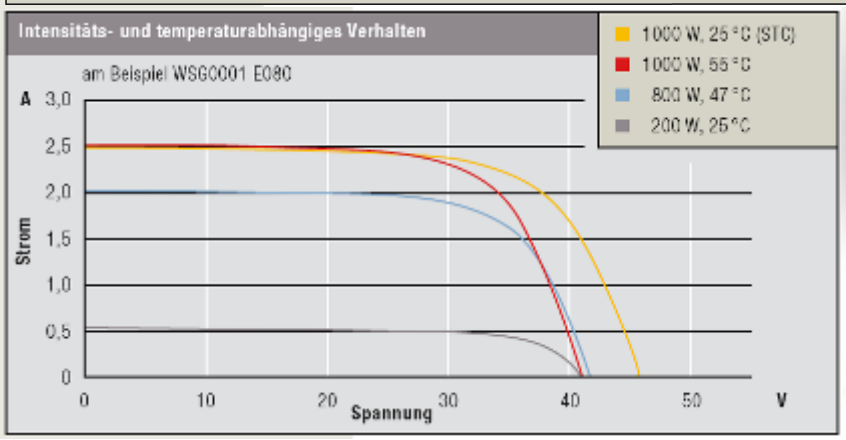

Figure 41: CIS modules by Würth

Appendix C Protective gas atmosphere

C.1 Introduction

The idea of using a protective atmosphere is widely applied in insulation glass. Here, noble gasses such as Agron and even Krypton are applied, due to their lower conductivity compared to air.

Gas	Molecular weight	Thermal conductivity (20 °C, 1 atm)
	g/mole	W/mK
Oxygen (O_2)	32	0.026
Nitrogen (N_2)	28	0.026
Argon (Ar)	40	0.017
Dry atmospheric air	29	0.026
Krypton (Kr)	84	0.010
Xenon (Xe)	131	0.006
Cyclopentane* (C_5H_{10})	70	0.012

*CYCLOPENTANE IS A WIDELY USED BLOWING GAS FOR POLYURETHANE FOAM.
TABLE 1. OVERVIEW OF MOLECULAR WEIGHT AND THERMAL CONDUCTIVITY FOR DIFFERENT GASSES.

Table 22: Thermal conductivity for different gasses (Hadorn, 2005).

Furthermore, the insulation can be improved further by lowering the pressure in the casing, as shown in Figure 42.

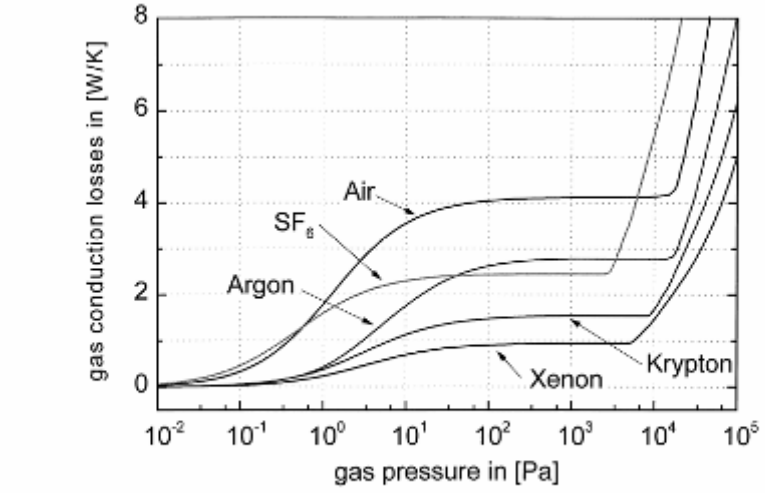

Fig. 2. Heat losses by gas heat conduction from the hot absorber to the casing in a flat-plate collector in dependency of the gas pressure in the collector casing for different filling gases. The typical operation pressure ranges in the plateau between 100 and 10^{-1} Pa.

Figure 42: Thermal conduction as a function of gas pressure (Benz and Beikircher, 1999).

Efforts to seal solar thermal collectors also have a long history. In 1980, a report was published by Mendelsohn on Collector sealants and breathing, in which a large amount of sealants was tested. Fluorocarbon was found as the most durable sealing material, with silicones as second best. Also, a number of adsorptive materials were tested for removing moisture and organic vapour from the collectors. Silica gel and activated carbon turned out to give the best results. Finally, the pressure increase in the collector cavity with the heating of the collector was mitigated by means of an external bladder underneath the collector.
From the same year, a publication by Zernial was found on the development of a selective thin film and of a hermetically sealed flat plate solar collector with gas filling. However, the only recent commercial

collector products found in this field are the gas-filled collector by Buderus and the flat-plate evacuated collector by Thermosolar, as described below.

C.2 Buderus

Buderus now has a commercial collector (type SKS 4.0) in which an argon atmosphere is applied. The inner space is sealed by means of stainless steel combined with butyl rubber. The edges have been sealed with silicones. The outer casing is made of glassfiber, thereby reducing weight and corrosion problems. The manufacturer indicates that additional advantages are that the sealing protects the collector from dust and also moisture, which prevents condensation inside the collector.

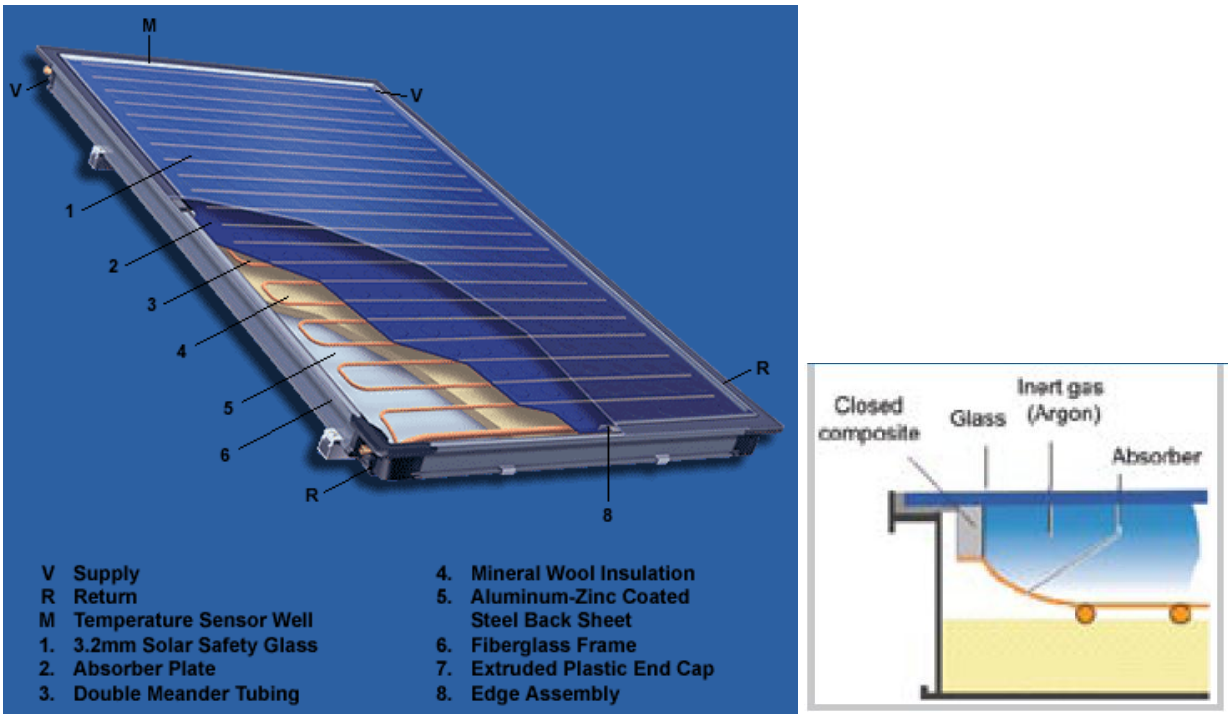

Figure 43: Buderus SKS 4.0 collector.

As additional information, an interview with Buderus is displayed from a journal.

"Der hermetisch dichte Randverbund zwischen Glas und Absorber wiederum verhindert, dass Feuchtigkeit in den Zwischenraum eindringt. Vorteil: Das Glas beschlägt in den Morgenstunden nicht, und der Sonnenkollektor bringt von Anfang an eine hohe Leistung. Außerdem ist die Absorberbeschichtung vor Schmutz und Umwelteinflüssen geschützt und läßt so eine durchweg hohe Leistung erwarten. Der Zwischenraum ist mit dem Edelgas Argon gefüllt, das die Wärmeverluste über die Glasscheibe reduziert." "Dafür sorge das Edelgas Argon im Innenraum, der mit Hilfe eines Edelstahl-/Butyl-Dichtungssystems dauerhaft und hermetisch abgeschlossen sei."
Der Rahmen besteht bei Buderus-Sonnen-kollektoren aus glasfaserverstärktem Kunststoff (GfK) – das hat gleich mehrere Vorteile. GfK ist gut 20 Pro-zent leichter als Aluminum und in der Verarbeitung weitaus flexibler. „Glasfaserverstärkter Kunststoff lässt sich extrem stark biegen und bleibt dabei dennoch formstabil", nennt Wenisch die Vorzüge. GfK ist zudem witterungs- und korrosions-beständig, was bei der extremen Belastung – große Temperaturunter-schiede im Sommer und im Winter – bedeutsam ist. Bei der Montage macht sich das geringere Gewicht bezahlt, denn der Einbau auf dem Dach ist dadurch einfacher. Heizungsfachmann ist über jedes Ki-logramm froh, das er nicht schleppen muss." Ein Sonnenkollektor Logasol SKS 3.0 wiegt nur 47 Kilogramm und ist damit leichter als vergleichbare Produkte mit Aluminumrahmen. Auf einem Montagetisch liegt ein neuer Rahmen, ein Mitarbeiter setzt gerade den Absorber ein.DerPass-genauigkeit hat oberste Priorität, schließlich müssen die einzelnen Komponenten am Ende ein Produkt wie aus einem Guss ergeben. Auch die Abdeckung aus extrem belastbarem Einscheiben-Sicherheitsglas schließt millimetergenau mit dem Rahmen ab. „Jede Scheibe wird gereinigt und getrocknet", erklärt Wenisch. Weder Schmutz noch Feuch-tigkeit dürfen die Funktion des Son-nenkollektors beeinträchtigen. Das ist besonders wichtig, weil der Logasol SKS 3.0 hermetisch abgedichtet wird – wiederum ein typisches Merkmal von Buderus-Sonnenkollektoren. Wenn Glasscheibe und Absorber in den Rahmen eingelassen und befe-tigt sind, füllt ein Mitarbeiter Argon in den Zwischenraum. Das Edelgas ist schwerer als Luft und drückt diese einfach aus dem Kollektor. Danach werden die Ränder mit Silikon verklebt, das Produkt hermetisch abgedichtet. Das hat mehrere Vorteile: Die Sonnenkollektoren ziehen keine Feuchtigkeit und sind so immer leistungsfähig. Anders als belüftete Sonnenkollektoren, deren Scheibenmorgens häufig mit Wasserdampf beschlagen sind und die zuerst von der Sonne getrocknet werden müssen, bevor sie ihre volle Leistung bringen.

Inzwischen ist das Silikon ausgehärtet, das überschüssige Material mit einem Spezialmesser entfernt. Kopfüber liegt der Sonnenkollektor am nächs-ten Bearbeitungsplatz. Dort wird Mineralwolle zur Dämmung eingebracht sowie die rückwärtige Kunststoffabdeckung montiert – und fertig ist das innovative Produkt.

C.3 Thermosolar

The Thermomax website states the following: "Due to the atmospheric pressure and the technical problems related to the sealing of the collector casing, the construction of an evacuated flat-plate collector is extremely difficult. To overcome the enormous atmospheric pressure, many internal supports for the transparent cover pane must be introduced. However, the problems of an effective high vacuum system with reasonable production costs remain so far unsolved."
However, recently flat-plate vacuum collectors have been developed, especially for medium-temperature industrial applications by the company Thermosolar. On their website (www.thermosolar.sk/aa-eng.htm), they indicate the following: "The company THERMO/SOLAR Žiar s.r.o., one of leading European manufacture for thermal solar collectors, was founded on 1.01.1992. [..] In 1997 we began to manufacture an advanced type of evacuated flat plate collector, which for today is the only collector of this type in the world. Its basic advantage is the high efficiency at higher working temperatures by a rather small capital expenses in area. Its assignment is to produce industrial heat and space heating for buildings."

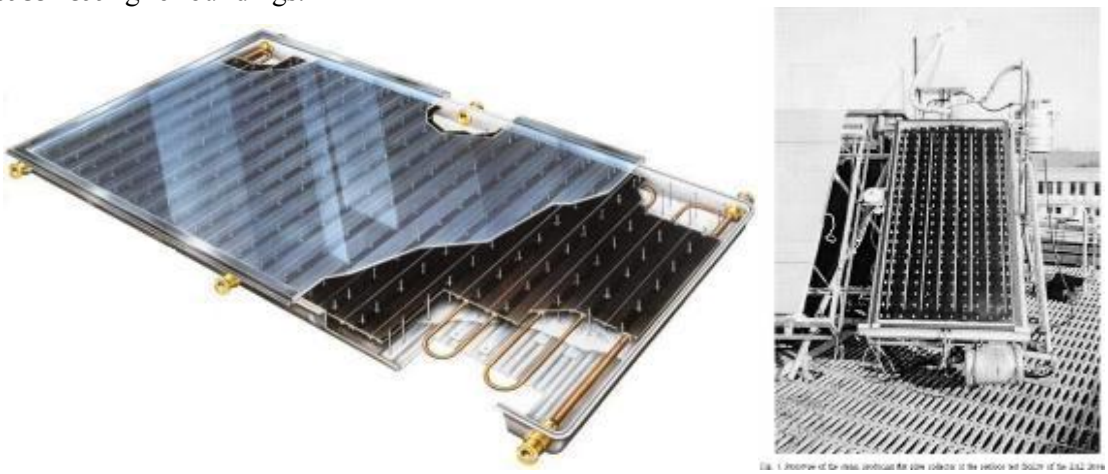

Figure 44: (a) Flat-plate vacuum collector Thermosolar (b) prototype flat-plate vacuum collector ZAE (Benz, 1999).

On their evacuated flat-plate collector (type TS 400V), the following claims are made: 'a unique evacuated flat plate collector produced in an industrial way. It is intended for installations in which the working temperature is more than 80 °C. The vacuum (insulation) guarantees stable operating parameters during the life of a collector.'

A similar (and possibly related) development was taking place at ZAE. Unfortunately, the information on the tightening system is limited to: "The identification of the parameters yielded extremely low loss coefficients in the range of evacuated tube solar collectors, although only a coarse vacuum with a low-cost tightening technique has been applied." (Benz and Beikircher, 1999).

Appendix D Unencapsulated PV

In R&D on new PV concepts, several parties are working on unencapsulated PV. The idea of this concept is that the PV is sealed from its environment by two glass plates, that are sealed around the edge to prevent intrusion of moisture and dust.

At Lenhardt Mschinenbau a production unit for unencapsulated CIS was developed as shown in Figure 45. Here, CIS modules are produced by connecting a CIS-coated glass plate to a normal glass plate by means of a frame as in insulation glass. The frame is not made of aluminium, but of a sprayed plastic (TPS – thermoplastic spacer). The space between the glazings is filled with argon and sealed finally with silicones.

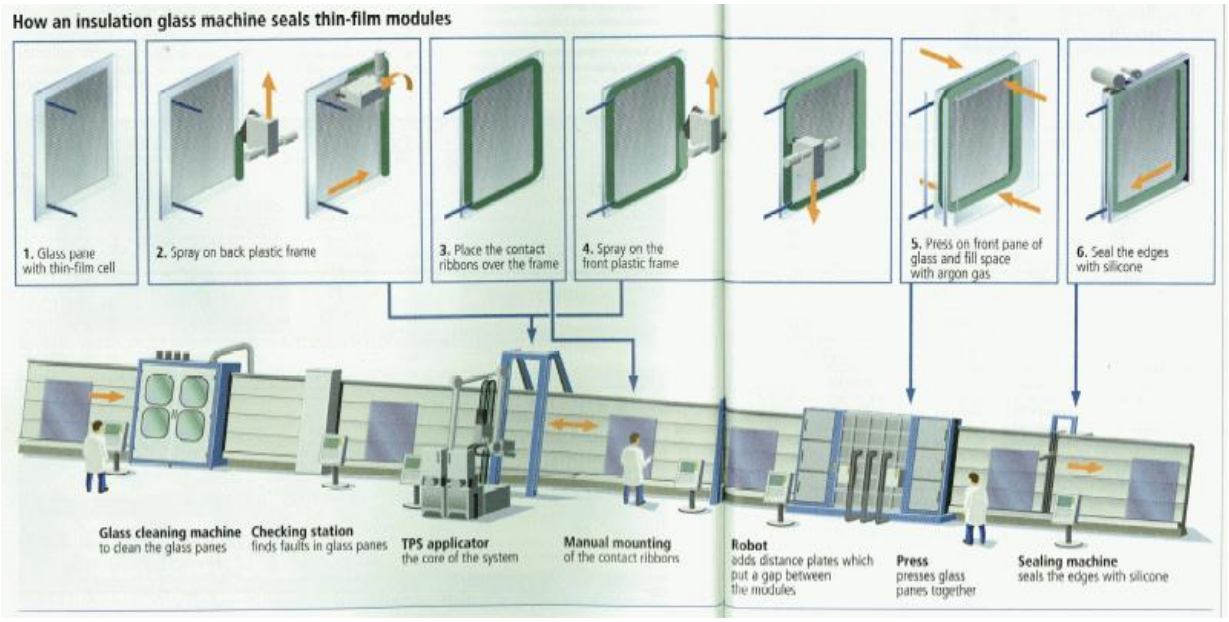

Figure 45: Production process of unencapsulated PV modules at Lenhardt Maschinenbau GmbH (Photon International, July 2007).